

Chapter 5

Hardfacing for Wear, Erosion and Abrasion

E. Badisch and Manish Roy

5.1 Introduction

Weld overlay coatings also known as hardfacing is a method which involves solidification for applied coatings. This method is as old as welding process and was first applied by J.W. Spencer in 1896. This technique offers unique advantages over other processes in that the overlay/substrate weld provides a metallurgical bond which is not susceptible to spallation and can easily be applied free of porosity and other defects. Weld deposits can have a thickness as high as 10 mm. Hardfacing process can be carried out easily even in on site. The process is also extremely versatile as a large variety of materials can be deposited for protection against degradation.

Weld overlay coatings can be classified under four different categories. These are (1) surface cladding where a thick layer of materials is applied and the overlay layer can have completely different composition from the substrate, (2) hardfacing where a materials more resistant to degradation is applied with good metallurgical bonding and the composition can be close in terms of composition to that of the substrate, (3) build up where a weld deposit is applied to restore the original dimension of the component and the composition of the build layer is exactly similar to that of the substrate and (4) buttering where an intermediate layer is deposited before applying the final coating.

The materials used for hardfacing should have melting point close to or lower than the substrate materials. During hardfacing, the temperature of the coating

E. Badisch (✉)
Austrian Center of Competence for Tribology, Viktor Kaplan-Strasse 2,
2700 Wiener Neustadt, Austria
e-mail: badisch@ac2t.at

M. Roy
Defence Metallurgical Research Laboratory, Kanchanbagh, Hyderabad 500058,
Andhra Pradesh, India

material is increased to the melting point and then allowed to solidify on the substrate. The effectiveness of hardfacing depends on the process of application of the hardfaced layer and the composition of the said layer. The process should be optimised to have high deposition rate, high thermal efficiency, excellent dilution, excellent control of composition and coating thickness.

The present chapter is concerned with various hardfacing processes, their advantages and disadvantages and finally the tribological performances of hardfaced surfaces, along with their high temperature properties.

5.2 Analytical Model for Heat Flow Equations

In order to balance the heat flow in an element, it is to be assumed that

Heat in–heat out = heat accumulated + heat generated. This can be represented mathematically as

$$-\frac{U}{\alpha} \Delta T + \Delta^2 T - \frac{1}{\alpha} \frac{\partial T}{\partial t} = -\frac{H}{k} \quad (5.1)$$

For one-dimensional heat flow model, it is assumed that heat flows in one direction and there is no convection or heat generation leading to the equation

$$\frac{\partial^2 T}{\partial z^2} = \frac{1}{\alpha} \frac{\partial T}{\partial t} \quad (5.2)$$

If it is assumed that the heat input is constant, thermal properties are independent of temperature, no heat loss due to convection and no latent heat effect, then the boundary conditions are

at $z = 0$, surface power density F_0 is given by

$$F_0 = \left(\frac{P_{\text{tot}}(1 - r_f)}{A} \right) = -k \left[\frac{\partial T}{\partial z} \right]_{\text{surf}}$$

at $z = \text{infinity}$

$$\frac{\partial T}{\partial z} = 0$$

At $t = 0$, $T = T_0$

Hence the solution is as given below:

$$T_{z,t} = \frac{2F_0}{k} \left\{ (\alpha t)^{1/2} \text{ierfc} \left[\frac{z}{2(\alpha t)^{1/2}} \right] \right\} \quad (5.3)$$

where ierfc is “integral of the complementary error function”.

When there is no heat source, the material will cool for $t > t_1$ according to the relationship given by

$$T_{z,t} = \frac{2F_0}{k} \alpha^{1/2} \left\{ t^{1/2} \operatorname{ierfc} \left[\frac{z}{2(\alpha t)^{1/2}} \right] - (t - t_1)^{1/2} \operatorname{ierfc} \left[\frac{z}{2(\alpha(t - t_1))^{1/2}} \right] \right\} \quad (5.4)$$

where T is temperature, z is depth, t is time, t_0 is the start time of heat source, t_1 is the end time of heat source, k is thermal conductivity, α is thermal diffusivity and F_0 is absorbed power density. This one-dimensional heat flow equation is applicable when the heat source is large compared to the depth considered. This solution does not take care any variation in beam size structure, speed or substrate thickness. Still solution of this model is useful, Brien and Kear [1] developed graphs of cooling rates, thermal gradient, solidification rates expected from this model.

The governing equation for the conduction of heat during hardfacing assuming no heat loss due to convection or radiation is [2]

$$\left(\frac{\partial^2 T}{\partial x^2} + \frac{\partial^2 T}{\partial y^2} + \frac{\partial^2 T}{\partial z^2} \right) = \frac{1}{\alpha} \frac{\partial T}{\partial t} \quad (5.5)$$

For a stationary instantaneous point source of energy $Q\rho C$, the solution for the above equation is

$$T = \frac{Q}{8(\pi\alpha t)^{3/2}} \exp \left\{ - \left[(x - x')^2 + (y - y')^2 + (z - z')^2 \right] / 4\alpha t \right\} \quad (5.6)$$

For a continuous point source, if heat is liberated at a rate of $\phi(t)\rho C$ from $t = 0$ to $t = t'$, then temperature distribution can be found by integrating the Eq. (5.5) over the time period as

$$T = \frac{1}{(8\pi\alpha)^{3/2}} \int \phi(t') \exp \left[\frac{-r^2}{4\alpha(t - t')} \right] \frac{dt'}{(t - t')^{3/2}} \quad (5.7)$$

where $r^2 = (x - x')^2 + (y - y')^2 + (z - z')^2$.

When $\phi(t)$ is constant and equal to q

$$T = \frac{q}{4\pi\alpha r} \operatorname{erfc} \left[\frac{r}{(4\alpha t)^{1/2}} \right] \quad (5.8)$$

More often than not the heat source during welding operation is a finite source with Gaussian heat distribution. In that case for stationary source temperature distribution is obtained as

$$T_{\text{cont-gauss}} = \frac{2P(1-r_f)D}{\pi D 2kT^{1/2}} \tan^{-1} \left[\frac{2(\alpha t)^{1/2}}{D} \right] \quad (5.9)$$

As the heat source moves during hardfacing at a velocity of v m/s the solution for temperature distribution becomes

$$T - T_0 = \frac{Q}{2\pi k} e^{-vx/2\alpha} \frac{e^{-vR/2\alpha}}{R} \quad (5.10)$$

The above equation appears to be most applicable analytical solution for hardfacing to find temperature distribution, cooling rate and heat affected zone, etc.

5.3 Hardfacing Processes

Most welding processes can be used for hardfacing. These processes can be grouped as torch processes, arc welding process and high energy beam processes.

5.3.1 Torch Process

Oxy fuel welding (OFW) and oxyacetylene welding (OAW) are the oldest and simplest torch hardfacing process which involves simply heating the surface with the flame until the surface is glassy and on the verge of melting and then melting the filler rod or powder to get the hardfacing to the melt. The filler rods or powders are heated until droplets from them wet the surface and form a continuous deposit. These processes are most widely used for cobalt, nickel and copper base hardfacing alloys. Although fuel gases other than acetylene can be used, most recommended gas is acetylene. These processes are one of the slowest processes but one which requires minimum alloy dilution. Since the process is slow, it is used for small jobs or where field welding torch is only available equipment. Usage of these processes requires welders with high skill. These processes have drawback that the base metal surface picks up carbon from the reducing flame.

5.3.2 Arc Welding Process

In the arc welding process, heat is generated by striking an arc between the electrode and the work piece [3]. Arc welding process can be grouped as consumable electrode process and non-consumable electrode process. In the consumable arc welding process, arc is maintained between a consumable electrode and the

work piece. In shielded metal arc welding (SMAW), weld overlay is deposited by melting a consumable wire covered by flux in an arc. The flux forms a liquid slag upon melting and the gas protects the molten metal pool. The electrode is made of an alloy or coating materials that forms wear-resistant deposit. The main advantage of this process is ready availability of the equipments and consumables even in small quantities. A large variety of ferrous and non-ferrous materials can be deposited by this process. This process is very slow and hence small area can be covered. This process is also dependent on the manual skill of the operator.

In flux cored arc welding (FCAW) which is widely used since 1975, a metallic tubular electrode is filled with flux materials. The flux material volatilises and provides protective shielding to the weld pool. The coiled tubular electrode wire is fed through the gun and an arc is established between the wire and the substrate. Sometimes metal powder can also be added to the core materials to create an alloy weld deposit. Gas shielding can also be provided to reinforce shielding effect. This process can be used as semi-automatic or automatic process. This process is very fast. However, few alloys are available in the form of tube and these alloys are mostly ferrous. This process is mainly suitable for large area ferrous materials.

During gas metal arc welding (GMAW), the consumable wire electrode and the substrate are protected from the atmosphere by a gas fed axially with wire through welding gun nozzle. Deposition of the weld overlay can be accomplished by several methods. The wire can short against the wire and this process is called short-circuiting transfer or short arc. It is also possible to get the wire melt off without touching the work. This process is called globular transfer. Deposition can also be done by a process known as spray transfer which is preferred mode for out-of-position welding. This process is very fast, can be applied to large area and can be used to clad inside a large tank; a wide variety of materials can be deposited. Sometimes it is possible to carry out this process without the gas shielding known as open arc process.

Submerged arc welding (SAW) process is a fast process which uses consumable wire flux applied by ancillary equipment [4]. The arc is struck between the work and the filler wire. During welding, the arc is covered with granular flux fed through a hopper that follows the welding head. Using additives with the flux necessary alloys can be deposited. This process can be easily automated. It is a fast process. It is suitable for cladding a large area but it is used mostly for ferrous materials. This can be used for anything that can be positioned for flat welding process.

Among non-consumable welding process, gas tungsten arc welding (GTAW) and plasma arc welding (PAW) process are used extensively. Both processes involve a tungsten arc electrode and introduction of filler materials in the form of wire in case of GTAW and powder in case of PAW. In GTAW, arc is generated by striking a non-consumable W electrode with the work piece. Filler material is supplied by putting a bare rod manually in the arc or by using other devices which introduces bare wire in the arc. Any materials can be deposited by GTAW although the process is very slow especially in manual mode and only small area can be covered. This process produces a neat deposit which is an advantage on finished machine parts.

In PAW process, an inert gas is flowed through an electric arc in the welding torch. The filler material is melt by plasma flame for hardfacing. The temperature of the flame can be as high as 50,000 K giving the flame high penetrating capability. When the plasma flame is obtained by an arc between the work piece and the plasma gun, the process is called plasma transfer arc (PTA). In case the arc is maintained in the torch between the tungsten electrode and the water cooled nozzle, the process is called non-transferred arc plasma. In this process filled material is added by spool feeding of bare wire or powder into the arc zone. This process is very fast although the equipment cost is very high. Hardfacing by PAW requires minimum machining. There is no requirement of flux removal. Thin or thick layer can be deposited by this process. Low melting substrate can also be coated by this process. The PTA process exhibits enormous potential because the PTA overlays have a lower production cost and a higher productivity compared to thermal sprayed coatings, as well as easy operation and no need for any special surface treatment [5–7]. Furthermore, the PTA technique allows the production of high quality coatings (good metallurgical bonding and low level of porosity) consisting of metal matrix and carbide hard phases

5.3.3 High Energy Beam Process

Among high energy beam processes, laser hardfacing [8–10] and electron beam hardfacing are important [11–13]. Surface modification by laser is discussed in details in Chap. 7. Hardfacing by electron energy beam has been developed for many years and increasingly implemented for industrial applications [14–17]. In this process, electrons are generated by heating negatively charged filament (cathode) to its thermoionic emission temperature range and accelerating the electron by passing them through an electric field. The kinetic energies of these electrons are converted into heat which is used for depositing the surface layer on the substrate. Accurately controllable energy density, small beam size, accurate beam alignment, low heat input, pure environment are important features of electron beam surfacing which makes this process superior to many other hardfacing processes for several application. High cost of equipment, high running cost and several other shortcomings prevent extensive usage of this process. However, rapid development for the equipment of electron beam hardfacing, requirement of demanding quality of surfaces, economic benefit of the process lead to widespread use of this process in recent time.

5.3.4 Other Hardfacing Process

Friction surfacing is a recent hardfacing process [18] for depositing thick coating where the consumable is forced to move parallel to the surface and made to rotate

simultaneously under applied load. As a result a hot plasticized layer typically 1–2 mm thick, depending on the consumable material, is formed. The temperature of the layer is nearly 40 °C below its melting point. A high contact stress is required to avoid the formation of oxide layer between the substrate and the consumable. Aluminium, titanium, mild steel, tool steel, stainless steel, satellite etc can be deposited on a wide range of materials employing this process [19–21].

Electroslag surfacing is another hardfacing process which is similar to SAW [22, 23]. This process uses equipment similar to SAW primarily for strip cladding. Slag from particulate flux shields the process. This process has high rate of deposition and this process can be applied on flat as well as curved surfaces. Low heat input, small and uniform penetration of the base materials, low dilution, extra low carbon in the deposited layer are the main characteristics of this process. The regular deposit profile obtained by this process reduces the machining cost and sometimes no machining is required. There is no ultraviolet radiation in this process. It is difficult to surface the internal surfaces of tubes, etc., employing this process. There is a limitation of the strip size and the thickness of the substrate.

Pulsed electrode surfacing (PES) and its variants pulsed air arc deposition processes are high energy density microwelding processes [24–26]. These processes use short duration high current electrical pulses via discharge capacitance. There is very little distortion or metallurgical changes of the substrate materials. The surface layer is rapidly solidified forming a fine grain structure. The equipment is compact, simple and portable. It can be operated manually or can be integrated to machine tools. It is mainly used for treatment of cutting tools.

5.4 Hardfacing Materials

From metallurgical point of view, hardfacing materials can be classified in to several types [27, 28] although many other points should be considered during selection of hardfacing materials [29]

- Iron-based alloys
- Cobalt-based alloys
- Nickel-based alloys
- Copper-based alloys
- Carbides
- Composite materials
- Materials deposited by friction surfacing

5.4.1 *Iron-Based Materials*

Iron-based hardfacing materials constitute the bulk of the hardfacing materials [30, 31]. Due to low cost and moderate wear resistance, these materials are ideal for

large area coating of crushing, grinding and earth moving equipment. They are often used for restoration of surfaces. Following types of iron-based hardfacing materials are available for deposition of coatings.

- Pearlitic steel
- Austenitic steel
- Martensitic steel
- Cast iron

5.4.1.1 Pearlitic Steel

Pearlitic steel variety of hardfacing materials is actually low carbon weldable steel containing limited alloy addition. Normally submerged arc welding is used for depositing pearlitic steel primarily to surface the components on routine basis. The microstructure and mechanical properties of the weld deposit are controlled by controlling composition of the feeding wire and flux. In general, a finer microstructure giving better wear resistance is preferred [32]. Sometimes higher addition of alloying element can be made. But such situation requires faster cooling rate in order to get desired microstructure. However, it is also necessary to preheat the substrate in order to avoid cracking due to generation of thermal stress during cooling.

5.4.1.2 Austenitic Steel

Austenitic steel, Hadfield manganese steel is the most widely used austenitic variety of hardfacing materials. This steel contains 12–16 % Mn and up to 1 % C. The steel can retain completely austenitic microstructure on cooling, but this microstructure is metastable. This material typified EFeMn–C is extremely tough, wear and shock resistance. It is sensitive to plastic deformation. During abrasion, as the material deforms, austenite transforms to martensite due to plasticity induced transformation [33, 34]. This increases the work hardening rate of the steel and this in turn increases the wear resistance. This material with high work hardening capability and moderate yield strength is capable of responding plastically to abrasion and impact loading. This plasticity helps in dissipating energy, and in the process cracking and spalling of the coating is avoided [35].

However, there are some inherent problems associated with this material. Annealing or slow heating followed by cooling results in embrittlement of the material due to precipitation of carbides in the grain boundary. In order to avoid carbide precipitation, high interpass temperature is avoided. Another way of avoiding this embrittlement is to reduce impurities such as Sb, Sn, P, As, N, etc. High purity steel does not undergo embrittlement. This embrittlement can further be reduced by fast cooling through the critical embrittlement temperature. Si is also added to avoid embrittlement problem. During hardfacing, if the deposited layer is

diluted highly, it results in cracking as the diluted layer may not be stable austenite resulting in peeling of the layer. High dilution is avoided by selecting highly alloyed steel. Highly alloyed composition allowed the austenite to be stable even with high dilution. Austenitic manganese steel is not corrosion resistance. Because of embrittlement problem, they are not used at elevated temperature. These steels are difficult to machine. Hence they should preferably be used in as-deposited condition.

5.4.1.3 Martensitic Steel

The composition of martensitic steel is so chosen that the microstructure becomes martensitic after air cooling. Martensitic surface has generally less impact resistance compared to pearlitic or austenitic structure although it has higher hardness and abrasive wear resistance. However, the toughness of martensitic structure can be improved by appropriate tempering treatment. Martensitic coating is deposited by putting two layers in order to avoid dilution. If machining is required, three layers are deposited. Martensitic layers are susceptible to cracking due to thermal stress as it is cooled in air relatively fast to avoid austenitic formation. To avoid such cracking preheating of the substrate is carried out. Care should be taken during preheating. If heated beyond some temperature, the microstructure may not remain fully martensitic. Part of it may be transformed to austenitic.

When protection is required against wear in corrosive environment, martensitic stainless steel is used as protective layer. A typical composition for such layer is 0.3 (wt%) C, 12 % Cr, 0.8 % Mo, 0.6 % Mn, 0.6 % Ni and 0.5 % Si. This steel is austenitic at elevated temperature and transforms completely to martensite on slow cooling. Before application, this steel is usually tempered to 773–873 K. A low carbon variety of this steel which contains higher amount of Cr in addition to Mo, V and W, could improve the life of continuous caster rolls by as high as 50 % [36]. If the application is concerned with wear protection at elevated temperature, martensitic variety of tool steels is used. The coated components are cooled to ambient condition to ensure martensitic structure and subsequently tempered to 923 K. During tempering, various alloyed carbides precipitate resulting in increase in hardness. This phenomenon is known as secondary hardening and this helps retaining the strength at elevated temperature.

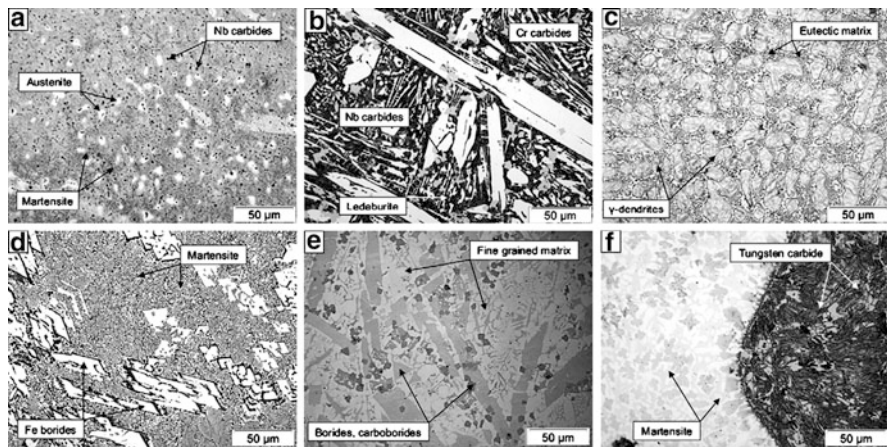
Six different hardfacing alloys produced as flux-cored wires on iron basis were selected and welded onto 1.0038 mild steel plates. The chemical compositions of these alloys are listed in Table 5.1 [37]. Table 5.2 shows the welding parameters, which are optimised related to the welding behaviour and the composition of the different flux cored wires. The welding was carried out in flat position in two layers. Typical microstructures of the welded deposits are shown in Fig. 5.1 [37]. Alloy A is mainly martensitic with some islands of austenite. Fine primary Niobium carbides are well distributed throughout the micro-section. The hardness of the martensite is about 800 HV0.1. The content of Nb carbides is given in Table 5.3 to 7 % at a size of <3 µm in a spattered shape. Alloy B consists of primary Fe/Cr

Table 5.1 Chemical composition of Fe base alloys

Alloys	Chemical composition					
	Fe	C	Cr	Nb	B	Others
A	Bal	<1.0	6.0	3.0	–	1.5
B	Bal	5.5	21.0	7.0	–	1.0
C	Bal	2.5	7.0	–	<1.0	<1.0
D	Bal	<1.0	–	–	4.0	1.5
E	Bal	1.3	15.4	4.2	4.2	11.5
F	Bal	–	<1.0	–	–	1.8

Table 5.2 Welding parameter of Fe based alloys

Alloys	Current (A)	Voltage (V)	Interpass temperature (°C)	Wire speed (mm/s)
A	175	22.9	168	4.4
B	247	27.5	197	8.4
C	246	21.7	205	5.4
D	188	23.3	182	4.7
E	244	23.6	175	9.3
F	113	21.0	151	3.0

**Fig. 5.1** SEM images showing the microstructures of various iron-based alloys [37]

carbides with a micro-hardness of roughly 1,600 HV0.1 in a ledeburitic matrix. The content of Fe/Cr carbides is listed in Table 5.3 to 57.1 % at a size of 30–200 μm. The chemistry of the Fe/Cr carbides is reported for hypereutectic FeCrC alloys in literature to M_7C_3 structure [38–41]. The hardness values of the ledeburitic matrix determined to be about 800 HV0.1, are close to previous investigations from Fischer [42] and Buytoz [43]. Besides, small and evenly distributed primary Nb carbides (light grey in Fig. 5.1b) at a volume content of approximately 5 % can be detected. These are supposed to be of major ingredient for increasing the resistance against erosion and abrasion due to their high hardness. Alloy C has solidified in

Table 5.3 Details of the hard phases (HP) of the Fe-based alloys

Alloys	Type of HP	Content of HP (vol.%)	Size of HP (μm)	Shape of HP
A	Nb carbides	7.0	<3.0	Spattered
B	Fe/Cr carbides	57.1	30–200	Columnar
	Nb carbides	5.4	<7.0	Granular
C	Fe/Cr carbides	48.3	–	Closed skeleton
D	Fe carbo-borides	18.5	20–80	Columnar
E	Fe/Cr carbo-borides	52.0	10–100	Columnar
	Nb carbides	4.6	5–10	Blocky
	Mo/W carbo-borides	5.3	10–25	Blocky
F	Synthetic WC	38.7	65–250	Rounded

hypoeutectic γ -dendrites with about 920 HV0.1, which are embedded in an eutectic matrix of about 1,000 HV0.1 (see Fig. 5.1c). A closed net or skeleton of brittle Fe/Cr carbides at a volume content of 48.3 % (see Table 5.3), is clearly surrounding the primary dendrites. This appearance comes close to a solidification of the finally solidifying eutectic melt described as N-type [42]. Alloy D is built up of Fe carbo-borides in columnar structure with a hardness of about 1,500 HV0.1 in a hard eutectic matrix of about 1,000 HV0.1 (see Fig. 5.1d). The distribution of hard phases in this alloy is quite uniform. Volume content and size of the Fe carbo-borides are listed in Table 5.3 to 18.5 % and 20–80 μm , respectively. The complex alloy E which contains an amount of boron similar to alloy D, but a much higher level of other elements like W, Mo, Nb and Cr and shows a dense and uniform distribution of very hard complex carbides and carbo-borides (see Fig. 5.3) with hardness values between 1,200 and 1,900 HV0.1. Type and content of the hard phases were determined to be Fe/Cr carbo-borides at a volume content of 52 % at a size of 10–100 μm , Nb carbides and Mo/W carbo-borides at a volume content of approximately 5 % in blocky shape. In ref. [44] hard phases of a very similar alloy are described as $\text{M}_{23}(\text{BC})_6$ and $\text{M}_7(\text{CB})_3$ carbo-borides phases in a matrix exhibiting high fracture toughness up to 73.3 $\text{MPa m}^{1/2}$ due to an effective distribution of fine carbide and boride phases in ductile dendrites/cells. The synthetic multiphase alloy F shows the original fused and crushed tungsten carbides (2,500–2,700 HV0.1) which are extensively dissolved in the Fe-based matrix and lead to well-distributed reprecipitated carbides with a decreased hardness of 1,200–1,600 HV0.1. Content and size of the synthetically added tungsten carbides is determined to be 38.7 % and 65–250 μm , respectively. The matrix has a hardness between 800 and 1,100 HV0.1. Higher welding amperage increases the rate of tungsten carbide dissolution. Overall the tungsten carbides are irregularly distributed. There is a higher density of original carbides close to the fusion line, whereas at the surface only rests of carbides are visible.

Wang et al. [45] produced a Fe-based alloy hardfacing coating reinforced by TiC particles. TiC particles were formed by metallurgical reaction of ferrotitanium (Fe–Ti) and graphite during the arc welding rather than the TiC particles being directly added into the welding pool. Figure 5.2 exhibits TEM image of lath martensite morphology of Fe-based hardfaced layer. TEM observation indicates

Fig. 5.2 The TEM micrograph showing martensite lath and the corresponding diffraction pattern of an iron-based hardfacing alloy reinforced with TiC [45]

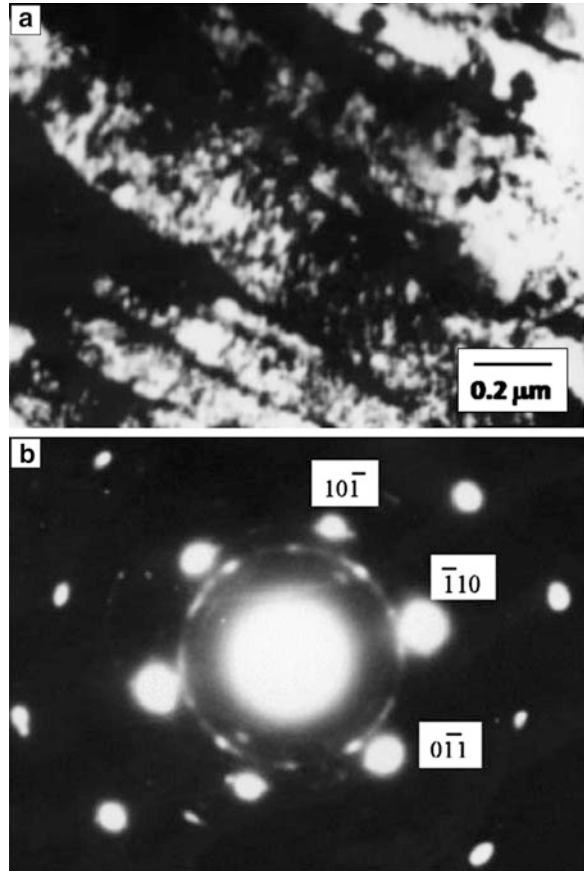
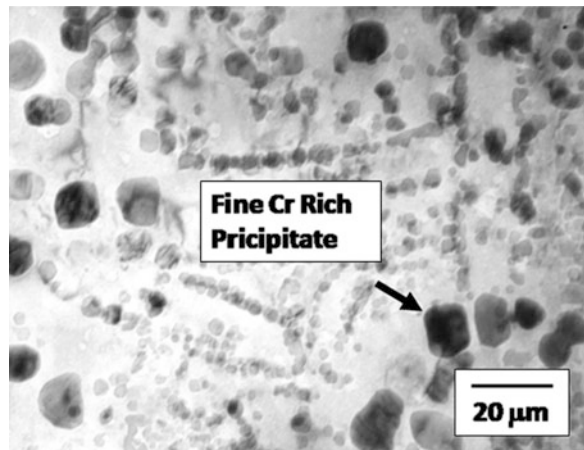


Fig. 5.3 TEM image shows the microstructure of Ni base alloy Colmonoy 5 [48]



that there is considerable dislocation in the subcrystal structure inside the lath martensite, but no twin martensite can be seen. The low carbon lath martensite has the features of auto-tempering. When low carbon lath martensite is formed, the microstructure of the hardfacing coating has a higher strength and the toughness is still largely maintained.

5.4.1.4 Cast Irons

Cast irons are essentially high carbon (usually more than 2 % C) containing iron. There are several varieties of cast irons available and these are obtained by changing the cooling rate, heat treatment and additives during cooling. Among these cast irons, white cast iron is used against wear protection. One variety of white cast iron which contains 12 % Cr is popular as hardfacing cast iron. Depending on the amount of carbon and Cr present, the hardfaced layer can be classified as hypoeutectic (2–3 % C, 5–29 % Cr), near eutectic (3–4 % C, 12–29 % Cr) and hypereutectic (4–7 % C, 15–36 % Cr) alloys. In general, hypereutectic alloy has higher abrasion resistance and lower impact resistance than hypoeutectic alloy. This high wear resistance is due to presence of high volume fraction of hard high chromium carbide [46]. These alloys contain various types of carbides mainly M_7C_3 types although other variety of carbides such as M_6C and M_3C are also available. The sizes of primary carbides are between 50 and 100 μm whereas the sizes of eutectic carbides are generally less than 10 μm [47]. Matrix surrounding these carbides can be pearlitic, austenitic or martensitic. Martensitic matrix is good for high stress abrasion resistance whereas austenitic matrix is preferred if wear resistance along with high fracture toughness is required [27]. Sometimes Ti, Nb and Mo are added to produce fine dispersed hard carbides. Such fine dispersion enhances the abrasion resistance along with toughness. This also leads to improvement of low stress and high stress abrasion resistance [38].

These alloys can be deposited by GTAW, FCAW, SAW and SMAW, etc. these alloys are one of the lowest cost hardfacing materials. Their overall wear performance is excellent and they can be used under variety of tribological degradation conditions. They have good availability and good applicability.

5.4.2 Nickel Base Alloys

These families of hardfacing alloys are used primarily for wear-resistant application. Boron is the main alloying element in these alloys. These alloys cannot be hardened by heat treatment. Further, these alloys are generally used in as-deposited condition. For similar hardness range, these alloys are more wear resistant than iron-based alloys. Physical and corrosion characteristics of these alloys are similar to Ni base alloys. These alloys are not ferromagnetic. They can retain their hardness up to 800 K. They cannot be formed at ambient condition and can be considered to

be brittle. These materials can be applied very easily and they can wet ferrous-based materials and other substrate better than most nonferrous hardfacing alloys. They can be machined more easily than other hardfacing materials with comparable hardness. These alloys can be classified under three heads.

- Boride-containing alloys
- Carbide-containing alloys
- Laves phase-containing alloys

Boride-containing alloys are available as bare cast rod, tubular wires and powders. The microstructure of this coating consists of borides and nickel borides in Ni-rich matrix. Nickel boride (Ni_3B) is the main hard phase at low chromium content. With increase in chromium content, nickel boride is gradually replaced by chromium boride. At low chromium content, chromium boride is CrB and at higher chromium content it is Cr_5B_3 . Si is an important matrix element which functions mainly as self-fluxing element and remains as an intermetallic compound Ni_3Si . The matrix also contains complex carbides such as M_{23}C_6 and M_7C_3 . These materials have least corrosion resistance compared to all non-ferrous hardfacing materials. They, however, have good high temperature hardness. A typical TEM bright field image of Ni base-hardfaced alloy Colmonoy 5 is shown in Fig. 5.3 [48]. The TEM bright field images of the coating showed needle (5–20 μm), fine spherical (20–200 nm), cuboidal (50–200 nm), blocky (2–3 μm) and floret (15 μm)-type precipitates TEM-EDS analysis confirms that the needles, floret blocky and fine spherical precipitates are basically rich in Cr with Ni and Fe as minor elements. Row of fine spherical precipitates of about 100 nm in size were observed (of about 1 μm length) as seen in Fig. 5.3. It has been reported that the Colmonoy 5 deposit can withstand its as-deposited hardness to the large range of temperatures [49]. These precipitates are beneficial to withstand high temperature hardness of the coating.

Carbide-containing alloys have excellent resistance against abrasion, galling, impact and corrosion. In these respects, these alloys are better than boride-containing Ni base materials. These alloys also contain complex carbides such as M_7C_3 and M_6C . Co-based hardfacing alloys were found to be sources for radioactive co isotopes [50], and hence carbide-containing nickel base alloys were developed.

Laves phases are essentially intermetallic compounds with general formula AB_2 . Although these phases improve the wear resistance, they generally bring down the toughness. Laves phase-containing Ni base alloys have less wear resistance than laves phase-containing Co base alloys. These laves phases are NiMoSi and $\text{Ni}_3\text{Mo}_2\text{Si}$. Generally laves phases constitute around 50 % of volume of the hardfacing layer. The structures of laves phases are hexagonal and dihexagonal [51, 52]. These alloys contain Cr for oxidation resistance. These alloys have good high temperature corrosion, oxidation and hot corrosion resistance. It has good metal to metal wear resistance especially at elevated temperature [53, 54]. They can be easily deposited by GTAW and PTA process. Since these alloys are devoid of Co, these alloys find application in valve and valve seat of nuclear reactor.

5.4.3 Cobalt Base Alloys

Cobalt base hardfacing alloys are well established for a considerable time. The main advantage of these alloys is their excellent corrosion and oxidation resistance in addition to wear resistance and that is why they are successful in replacing iron-based alloys. These alloys are however more expensive than other variety of alloys. The first Co-based hardfacing alloy was developed as Stellite.

These alloys are also known as carbide-containing alloys. Subsequently other families of alloys were developed and they are known as Triboalloy. These alloys can be classified as laves phase-containing alloys. These alloys cannot be hardened by heat treatment and they do not respond to annealing. Co base hardfacing alloys are available as bare rod for GTAW and OAW deposition, as coated electrode for SMAW and as wire for GMAW, FCAW, SAW and PTAW.

Stellite alloys contain varying amount of carbon and tungsten or carbon and molybdenum to change hardness and other properties. The matrix is essentially cobalt strengthened by chromium and tungsten or cobalt strengthened by chromium and molybdenum. The wear resistance is governed by formation of carbide, their volume fraction and size and distribution. High chromium content leads primarily to chromium carbide formation. However, volume fraction, size, shape and distribution of carbides are controlled by the composition of the alloy and their deposition technique. Depending on the amount of carbon present, these alloys can be divided as hypoeutectic, eutectic and hypereutectic alloys. In hypoeutectic alloys, especially low carbon content variety, ductile chromium carbide in the form $M_{23}C_6$ is normally present. In some of the alloys, a network of eutectic $Co-M_7C_3$ is present. These alloys have limited ductility but exhibit improved wear resistance. The size, nature and distribution of the carbides can powerfully be influenced by addition of molybdenum [55]. Addition of molybdenum results in formation of two types of carbides, M_6C carbide primarily at the Co-rich dendrite interface and eutectic chromium-rich M_7C_3 and $M_{23}C_6$ in the interdendritic region. Further, molybdenum addition decreases the arm spacing of cobalt-rich dendrite arm spacing and the size of the chromium-rich carbides. Molybdenum addition also helps in improving the hot hardness of the layer. Figure 5.4a–d [55] shows optical micrographs of the etched cross section of the Mo-free Stellite 6 and Mo-modified Stellite 6 hardfacing alloys deposited by the PTA. The first phase to form during cooling from the liquid state of the Stellite 6 alloy produced by PTA process is the primary Co-rich dendrite and the remaining liquid eventually solidifies by a eutectic reaction into an interdendritic, intimate lamellar mixture of Co-rich phase and Cr-rich carbides.

It is mentioned earlier that laves phases are intermetallic compound. In case of cobalt base alloys, these phases are generally $CoMoSi$ or Co_3Mo_2Si . Wear behaviour is primarily governed by volume fraction of laves phases. These alloys have superior high temperature strength than carbide-containing alloys. Accordingly these alloys exhibit superior high temperature tribological properties. These alloys are not machinable.

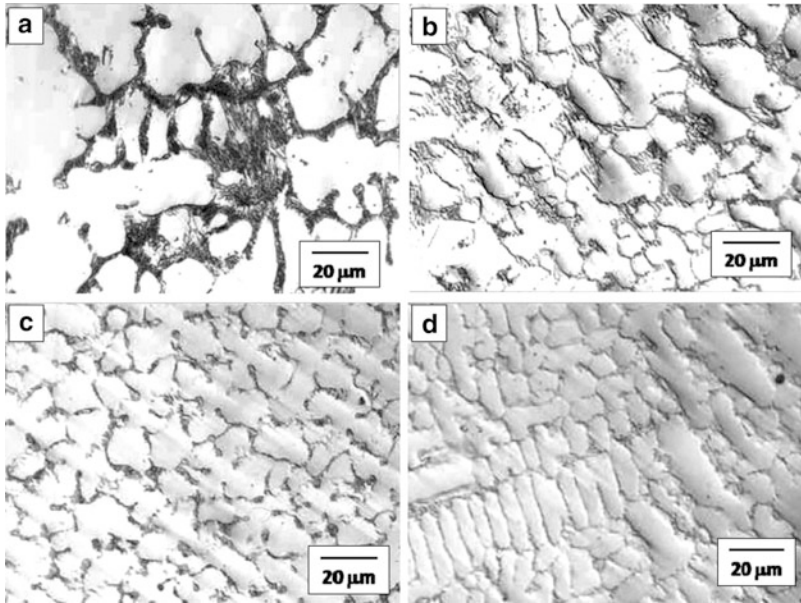


Fig. 5.4 Optical micrographs of cobalt base hardfacing alloys Stellite 6 containing increasing amount of Mo. (a) Mo free, (b) 1.5 % Mo, (c) 3 % Mo and (d) 6 % Mo [55]

5.4.4 Copper Base Alloys

Copper base alloys as various bearing materials are used in the industry for quite some time. Although these materials are well known as tribological materials, they are good for specific tribological condition. They are especially poor against abrasion. Copper base alloys can be classified under four categories as given below.

- Brasses, Cu–Zn alloys
- Aluminium bronzes, Cu–Al–Fe alloys
- Phosphor bronze, Cu–Sn–P alloys
- Silicon bronze, Cu–Sn–Si alloys

Brasses are single phase Cu–Zn solid solution alloy. This alloy cannot be hardened by heat treatment. This alloy is utilised in metal to metal contact wear applications. On the contrary, aluminium bronze can be hardened by forming martensite although hardfaced aluminium bronze is normally used as deposited condition. Other two varieties of alloys, namely phosphor bronze and silicon bronze cannot be heat treated. None of these alloys can be used for temperature in excess of 473 K. These alloys are available in the form of rod, small diameter wire and coated electrode and these alloys can be deposited by almost all available welding process for hardfacing. These alloys can be applied to ferrous, nickel and copper substrates.

5.4.5 Composite Materials

This category material contains carbides, nitrides or borides of tungsten, titanium, vanadium or chromium in very high proportion. Although tribological properties such as abrasion resistance or erosion resistance are found to improve by order of magnitude [56, 57], hardfaced layers produced by such materials suffer from the propensity of thermal fatigue and crack initiation at the interface of incoherent carbide and poor impact resistance. In general, wear performances improve with increasing volume fraction of hard phases. However, a detrimental effect of increasing the proportion of hard phase in the layer is decrease in fracture toughness at high volume fraction of carbides [58, 59]. Another limitation on the use of carbide-reinforced metal matrix composites has been dissolution of carbide in the matrix phase during deposition [60]. Intermetallic compounds such as $\text{Ni}_2\text{W}_4\text{C}$ formed by dissolution of WC were identified as a potential site for subsequent crack initiation [61]. During deposition of these materials especially WC-containing materials, care should be taken to prevent excess dissolution of WC. If dissolved in Co base or Ni base alloys, these carbides can reprecipitate as W_2C or η phase. W_2C and η phases are very brittle and they have inferior wear and corrosion resistance [62]. During processing of these materials, care should be taken to avoid excess welding current. If the excess welding current is employed during deposition, some of the wear resistance carbides may be dissolved. Some of the important varieties of composite materials are Stelcar[®] 1215 Stelcar[®] 60, Super Stelcar[®], etc. In recent years, a new type of hardfacing alloy with a very fine dispersion of carbide phases has been introduced in order to increase both fracture toughness and abrasion resistance [63, 64]. This range of hardfacing alloys has been described as nanostructured materials [64] and complex high alloy type of hardfacing deposits [64]. The high level of alloying additions (Nb, Cr, W and Mo) has enabled a significant undercooling of the melt prior to nucleation and solidification, resulting in a very strong refinement of the carbide phases and matrix. In addition, the alloying elements have acted to enhance the hardness of the carbide phases. The structure of these highly alloyed deposits has been identified as containing complex type precipitates in a matrix of either α -Fe or γ -Fe [64].

The XRD patterns of the Cr_3C_2 and Cr_3C_2 -Ni reinforced alloys and NiCrBSi matrix alloy are shown in Fig. 5.5 [65]. XRD analysis of the original NiCrBSi matrix alloy indicated a high amount of FeNi_3 solid solution in Ni-based matrix with presence of small amount of Ni_3B and Cr_7C_3 hard phases (Fig. 5.3a). When 40 vol.% Cr_3C_2 particles were added to the NiCrBSi alloy, Cr_3C_2 , Cr_7C_3 and M_{23}C_6 phases could be detected by XRD analysis in the hard phased layer as shown in Fig. 5.3b. Intensive dissolution of carbides results in an increased content of free Cr and C in the liquid alloy, which influences the matrix composition and leads to the formation of an austenite $\text{Ni}_{2.9}\text{Cr}_{0.7}\text{Fe}_{0.36}$ phase. The complex phase Cr_7C_3 is formed in the alloy as reprecipitated carbides during the rapid solidification process. It should be outlined that XRD peaks for many chromium carbides and borides are very closely placed and with significant alloying in these phases, confirmation of

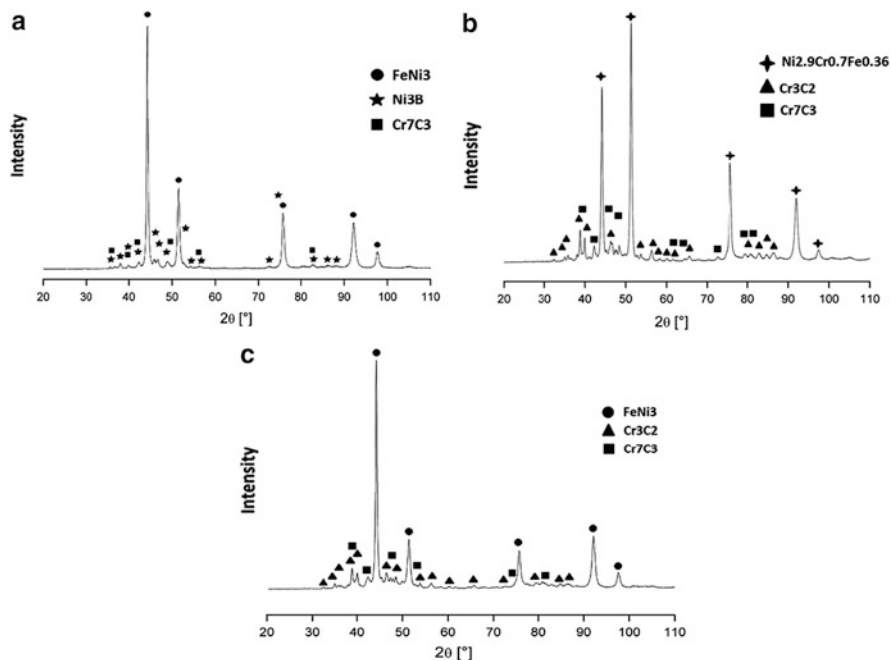


Fig. 5.5 The XRD patterns of the Cr_3C_2 and Cr_3C_2 -Ni-reinforced alloys and NiCrBSi matrix alloy [65]

the type of carbides from XRD alone is difficult. Therefore the presence of M_{23}C_6 phase is very doubtful. Almost all peaks of M_{23}C_6 match with Cr_7C_3 and Cr_3C_2 peaks. Furthermore, M_{23}C_6 phase is usually not formed by high free carbon levels and the microstructural analysis hasn't revealed any M_{23}C_6 carbides in the hardfacing matrix. Most probably those peaks correspond to some mixed Cr-B-Ni phase presented as precipitations in the matrix. Figure 5.5c presents the XRD analysis of the NiCrBSi alloy with addition of 40 vol.% Cr_3C_2 -Ni powder. In this case, due to the Ni binder in the cermet particles, the dissolution of chromium carbides is negligible and the matrix phase was identified as FeNi_3 with a high content of Cr_3C_2 and Cr_7C_3 hard phases. The presence of Cr_7C_3 can be explained by the structure of the precursor Cr_3C_2 -Ni bulk cermet, where a certain amount of Cr_7C_3 was formed during sintering.

Figure 5.6 illustrates the typical cross-sectional OM micrographs of composite coatings. The reference material (NiCrBSi self-fluxing matrix alloy) exhibits a nickel-rich dendritic matrix containing borides and carbides (Fig. 5.4a) that is a typical phase composition for alloys with low chromium content. According to phase distribution analysis, the content of Cr_7C_3 phase is 2 ± 1 wt%, whereas the content of Ni_3B phase is 19 ± 1 wt%. Figure 5.6b shows the microstructure of the Cr_3C_2 (Sulzer Metco 70C-NS) reinforced hardfacing layer. The micrograph reveals the presence of a high amount of re-precipitated spine-like carbides (Cr_7C_3)

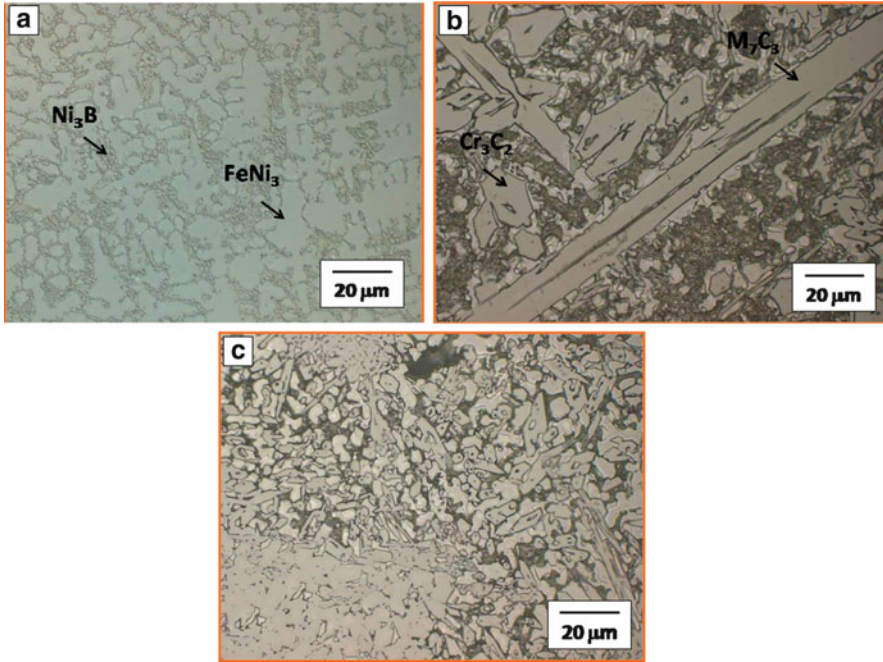


Fig. 5.6 OM cross-sectional images of composite materials: (a) NiCrBSi matrix; (b) Cr_3C_2 reinforced coating; (c) Cr_3C_2 -Ni reinforced coating [65]

resulting from the extensive carbide dissolution in the matrix. Figure 5.6c illustrates the microstructure of the coating produced from cermet powder in combination with NiCrBSi matrix. The microstructure of this coating can be characterised by three apparent phases: hard phases-rich hypereutectic matrix material, some amount of dissolved and re-precipitated Cr_7C_3 carbides and a certain content of particles of the initial cermet particles homogeneously distributed throughout the matrix. It is assumed that the nickel binder in the cermet particles protects the primary carbides from dissolution and helps keeping the particles in the original composition.

5.5 Tribology of Hardfaced Surfaces

5.5.1 Sliding Wear

Sliding wear behaviour of hardfaced surfaces is studied extensively. Comparative wear tests on a regular share and three kinds of hardfacing with electrodes were conducted by Bayhan [66]. The influence of different hardfacing electrodes on the

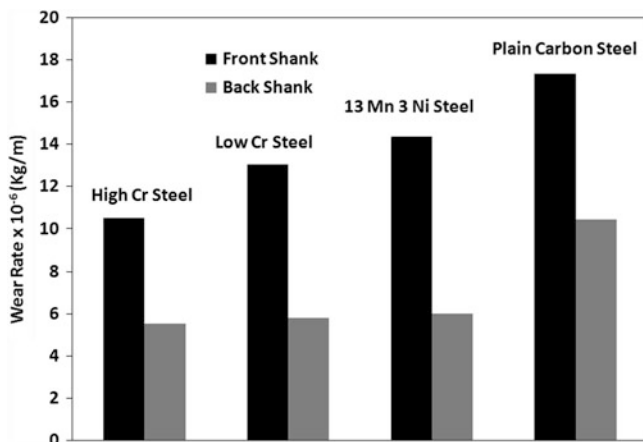


Fig. 5.7 The influence of different hardfacing electrodes on the wear rate of the share cutting edge of a chisel plough [66]

wear rate of the share cutting edge of a chisel plough is depicted in Fig. 5.7. It was found that the hardfaced share had a positive effect, as the hardness of the share cutting edge increased and the wear decreased. Su and Chen [67] deposited Ni base hardfacing layer on AISI 1045 steel and reported that addition of Nb reduced friction and wear loss. Addition of Mo and C resulted in formation of carbides with excellent wear resistance.

In a study by Wang et al. [68, 69], different hardfacing layers were produced by shield manual arc welding (SMAW) process in which a bare electrode of H08A was coated with fluxes, to which different measures of ferrotitanium (Fe–Ti), ferrovanadium (Fe–V), ferromolybdenum (Fe–Mo) and graphite had been added. The influence of added alloy elements on the microstructure and wear properties of the Fe-based hardfacing layers was investigated. The results showed that complex carbides of $TiC-VC-Mo_2C$ were synthesised via metallurgical reaction during hardfacing. Carbides are uniformly dispersed in the matrix. The addition of graphite and ferromolybdenum can enhance macro-hardness and wear resistance of the hardfacing layer significantly. However, it increases the crack sensitivity of the hardfacing layer. With the increasing of the additions of Fe–Ti and Fe–V, the macro-hardness and wear resistance of the hardfacing layers are increased. A good resistance against cracking and wear resistance of the hardfacing layer could be obtained, when the amounts of graphite, Fe–Ti, Fe–V and Fe–Mo were controlled within a range of 8–10 %, 12–15 %, 10–12 % and 2–4 %, respectively as shown in Fig. 5.8 [68]. The deposited layer surfaced by Fe–Ti–V–Mo–C hardfacing alloy possesses a higher wear resistance and less friction coefficient than that of the deposited layer surfaced by EDRCrMoWV-A3-15 hardfacing alloy.

Wang et al. [68] also recorded the features of worn surface of hardfacing layer containing increasing amount of Mo. Figure 5.9 [69] shows the SEM micrographs of the worn surface of the specimens containing increasing amount of Mo after

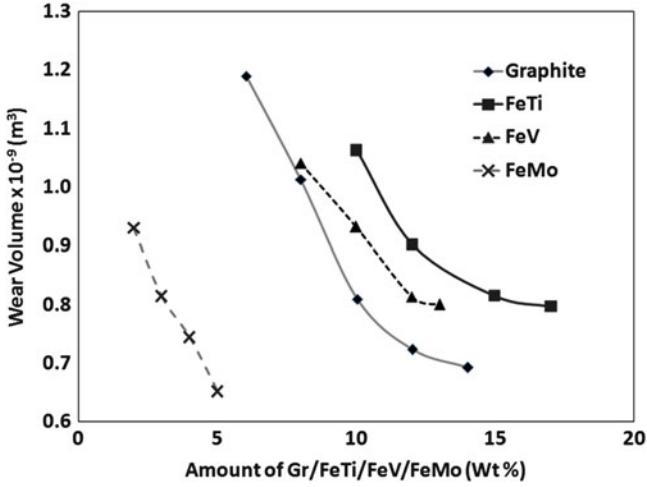


Fig. 5.8 Wear rate of the iron-based hardfacing layer when the amounts of graphite, Fe-Ti, Fe-V and Fe-Mo in the flux were controlled within a range of 8–10 %, 12–15 %, 10–12 % and 2–4 % [68]

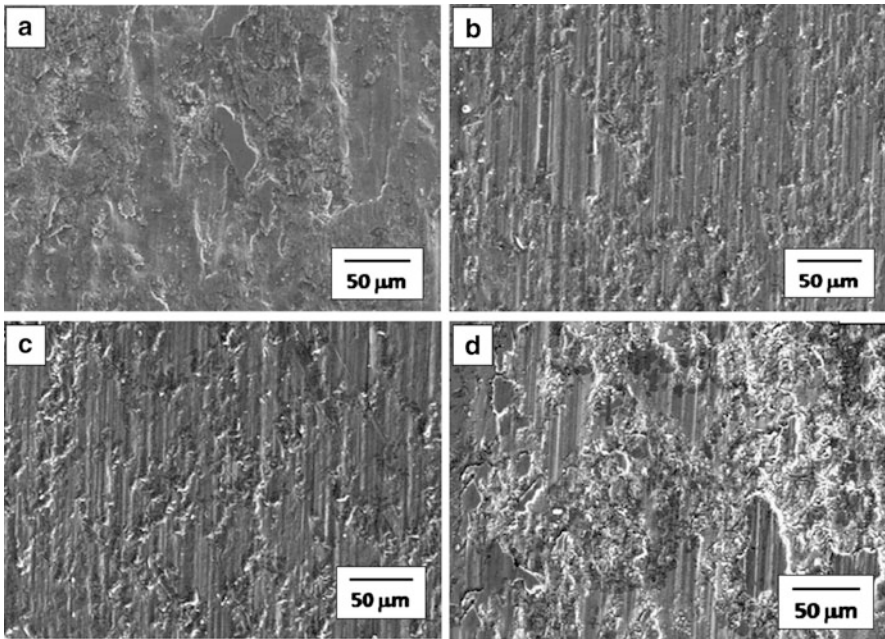


Fig. 5.9 SEM micrographs of the worn surface of the specimens containing increasing amount of Mo after wear test in air at normal load of 98 N and sliding distance 1,260 m [69]

wear test in air at normal load of 98 N and sliding distance of 1,260 m. Compared with the specimens containing higher amount of Mo (Fig. 5.9b–d), the worn surface of the Mo-free hardfacing layer (Fig. 5.9a) shows serious plastic deformation and deep groove. This results from the lower hardness and less volume fraction of carbide in the Mo-free specimen. However, for specimens containing Mo, the hardfacing layers exhibit relatively smooth worn surface, and there is no indication of brittle failure or loose debris formation of carbides. It indicates that hardfacing layers with Mo alloy possess a much higher resistance to plastic deformation and removal of the edges of grooves. In addition, it is found that some void formation at carbide/matrix interfaces and the fall-off of carbides in the specimen containing highest amount of Mo. Compared to wear scar of specimen containing highest amount of Mo, fall-offs of carbide of specimens containing lower amount of Mo are lower. It reveals that specimens with intermediate amount of Mo offer the best overall properties of wear and crack resistance.

Figure 5.10 shows the wear damage of a series of Co base and Ni base alloys deposited by gas tungsten alloy welding (Fig. 5.10a) and a series of cobalt base alloy Triboalloy deposited by plasma transfer arc welding (Fig. 5.10b) rubbed against a series of counter-body materials [28]. Wear rate is low when rubbed against Hastelloy C-276. It is generally high when the counter-body is 304 SS. The lowest wear rate is exhibited by ERCoCr-C alloy against Hastelloy although it has the highest wear rate against 304 SS. Wear rates of the alloys deposited by plasma transfer arc are generally lower than that deposited by gas tungsten welding. These data are obtained by using pin on block rig at an applied load of 2,722 kgf. Triboalloy T-400 has excellent galling resistance and it is particularly suitable when lubrication is not possible. In fact, under self-mated condition Triboalloy T-400 exhibits superior wear resistance than satellite 6. Triboalloy T-800 contains high amount of Cr and hence suitable for high temperature wear resistance. The wear properties of a series of satellite base alloys have been investigated by Foroulis et al. [70]. An excellent property especially in self-mated condition is noted. Such performance is due to low stacking fault energy of satellite coatings. The low stacking fault energy indicates less tendency for cross slip and this tendency, in turn, facilitates transformation from body centered cubic structure to hexagonal close packed (h.c.p.) [71] structure during deformation. During sliding, these hcp structures reorient themselves to have basal planes parallel to the sliding surfaces [72]. Basal plane sliding reduces the friction force to minimum. Further, there is significant strain hardening during deformation. Thus satellite creates a layer which combines low friction with high load bearing capacity.

A correlation was made among microstructure, high-temperature wear resistance and surface roughness in hardfacing alloys reinforced with complex carbides by Kim et al. [73] and Choo et al. [74]. The hardfacing alloys were deposited on a low-carbon steel substrate by a submerged arc welding method. Different fractions of FeWTiC and WTiC carbide powders were included inside hardfacing electrodes. Microstructural analysis indicated that cuboidal and rod-type complex carbides were homogeneously distributed in the bainitic matrix. As volume fraction of these complex carbides increased, hardness and wear resistance increased as shown in Fig. 5.11 [73]. The alloy reinforced with FeWTiC carbides contained

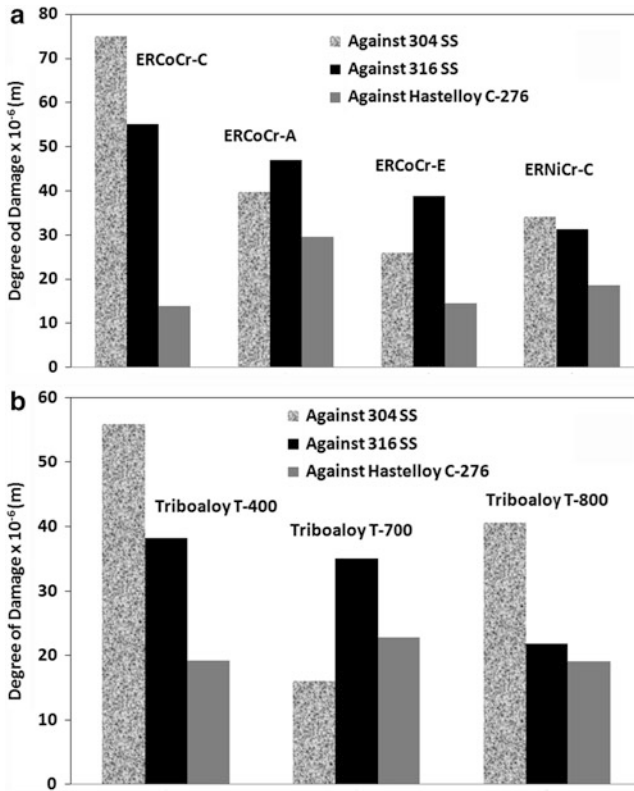


Fig. 5.10 The degree of damage of various (a) Co base alloys and (b) Triboalloy sliding against various counter bodies [28]

more complex carbides in the harder matrix than those reinforced with WTiC carbides because of efficient melting and solidification during hardfacing, and thus showed the best wear resistance and excellent surface roughness. Hardness, wear resistance and surface roughness of the hardfacing alloys reinforced with complex carbides were better than high speed steel rolls. In-situ observation of the fracture process showed that microcracks were initiated at complex carbides and that shear bands were formed between them, leading to ductile fracture. The hardness, wear resistance and fracture toughness of the hardfacing alloys reinforced with complex carbides were improved in comparison with high-chromium white-iron hardfacing alloys, because of the homogeneous distribution of hard and fine complex carbides in the bainitic matrix [75].

Relative wear resistance of a series of Ni base alloys is presented in Fig. 5.12. It is clear that the wear resistance of boride-containing alloys is lower than carbide-containing alloys. Among boride-containing alloys, colmonoy 6 has best wear resistance. Carbide-containing alloys have excellent and comparable wear resistance. Interestingly alloys containing tungsten also exhibit similar wear resistance.

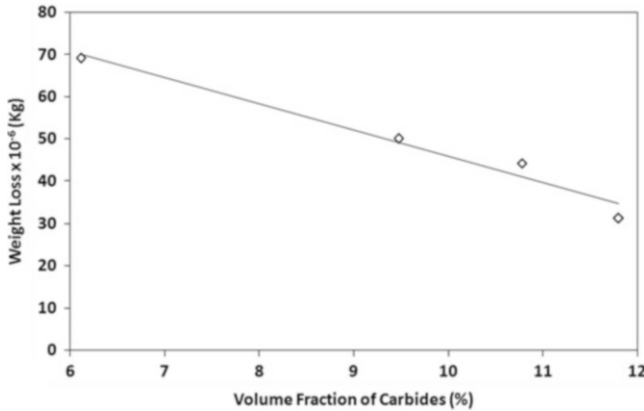


Fig. 5.11 Variation of wear rate as function of volume fraction of carbides of various iron-based composite alloys [73]

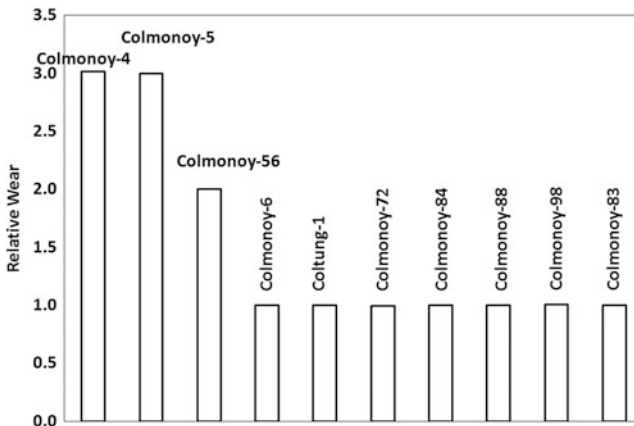


Fig. 5.12 Bar diagram showing the relative wear of a series of Ni base alloys

In another study by Wu and Wu [76], it is reported that Co based alloys deposited using plasma transfer arc are not suitable for low alloy steel. However, Ni base alloy deposited by PTA showed good performance.

Wear at elevated temperature for hardfaced materials has received considerable attention. Nichols [54] investigated a large number of hardfacing alloys for high temperature wear and noted that Triboalloy 700, 800 and Stellite 6, 12 and 20 are excellent coatings. In a study by Lee et al. [77], sliding wear behaviour of newly developed Fe-base Co-free hardfacing alloy (Fe–Cr–C–Si) was investigated and compared to that of Stellite 6 and Fe-base NOREM 02 in the temperatures ranging from 300 to 575 K under a contact stress of 103 MPa (15 ksi) using a sliding wear test apparatus installed in an autoclave filled with distilled water. The weight loss of Fe–Cr–C–Si was equivalent to that of Stellite 6 over all temperatures range in 100-

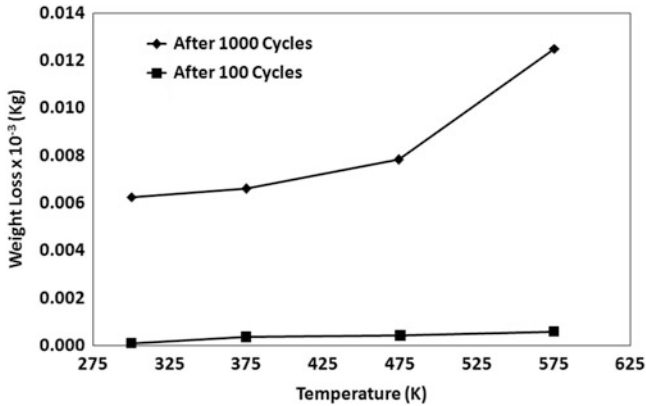


Fig. 5.13 Influence of temperature on the wear rate of newly developed Fe-base Co-free hardfacing alloy (Fe–Cr–C–Si) [77]

cycle wear test. The weight loss of Fe–Cr–C–Si 1000-cycle wear test increased almost linearly with increasing temperature up to 575 K as presented in Fig. 5.13. It is noted that for Fe–Cr–C–Si alloy, the tendency for oxidative wear resulting in the formation of glaze layers increased with increasing sliding distance and test temperature. Lee et al. [78] also noted that under pressurised water and up to 573 K, best wear resistance was exhibited by Fe–20Cr–1.7C–1Si alloy. This behaviour was primarily due to strain induced martensite transformation. Figure 5.14 gives the TEM images showing the transformation of the matrix to martensitic due to strain induced transformation [78]. The wear resistance of this alloy was comparable to that of satellite 6. The martensite was observed at the worn surfaces tested at the room temperature. TEM micrograph of the specimen before wear test showed no strain-induced martensitic transformation (Fig. 5.14). Therefore, external stress induced martensitic transformation and affected the wear behaviour. Kesavan and Kamaraj [48] examined dry sliding wear behaviour of nickel base hardfaced of nearly 4–5 mm thickness coating deposited using plasma transferred arc (PTA) welding process on 316 L (N) stainless steel substrate without any defects. Results showed that the wear resistance of coating improved significantly with increase in test temperature, and the high wear resistance was observed at 823 K.

5.5.2 Abrasive Wear

Maximum tribological work of hardfaced surfaces is done under abrasive wear condition [79–81]. The abrasive wear resistance is related to the hardness of the hardfaced layer. Interestingly microstructure also plays important role. Plain carbon-hardfaced steel alloys have different microstructures. In non-hardenable steel, ferrite is the matrix and hard phases can be carbide or cementite. In

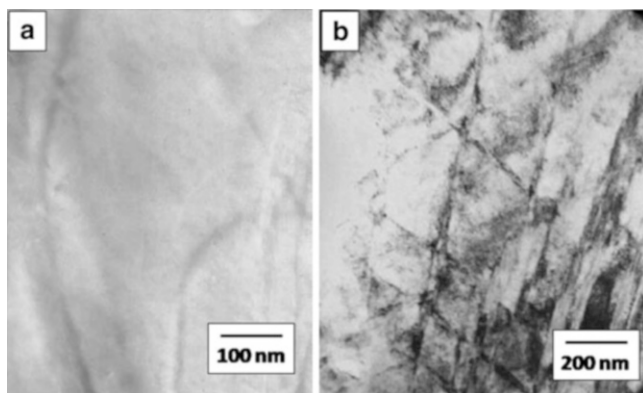


Fig. 5.14 TEM image showing martensite free and strain induced martensite in the matrix of Fe–Cr–C–Si alloy [78]

hardenable steel, matrix can be austenite with other hard constituent. In hardened condition it is martensite or bainite matrix. Figure 5.15 shows steel with similar hardness and different microstructure have different abrasive wear rates [81]. Clearly martensitic microstructure is the best for wear resistance application followed by bainitic microstructure. Interestingly they also have high hardness.

Hardfacing is one of the most useful and economical ways to improve the performance of components subjected to severe abrasive wear conditions. A study was made by Buchely et al. [82] to compare the microstructure and abrasion resistance of hardfacing alloys reinforced with primary chromium carbides, complex carbides or tungsten carbides. The hardfacing alloys were deposited onto ASTM A36 carbon steel plates by a shielded metal arc welding (SMAW) method. Three different commercial hardfacing electrodes were employed to investigate the effect of the microstructure. The abrasion tests were carried out in a dry sand–rubber wheel abrasion machine according to the procedure A of ASTM G65 standard. The results showed that the wear resistance is determined by the size, shape, distribution and chemical composition of the carbides, as well as by the matrix microstructure. The best abrasion resistance was obtained in microstructures composed of eutectic matrix and primary M_7C_3 or MC carbides, while the higher mass losses were measured in completely eutectic deposits. The main wear mechanisms observed at the surfaces included microcutting of the matrix and brittle fracture of the carbides.

When a contacting abrasive particle forms a groove by plastic deformation, volume of material removal can be represented as

$$\delta V = k_1 \times k_2 \times A \times S \quad (5.11)$$

where k_1 is the probability of materials removal, k_2 is the proportion of the groove volume that forms wear debris, A is the cross-sectional area and S is the sliding distance. The cross-sectional area of the groove is related to the depth of indentation of the particle p^2 as

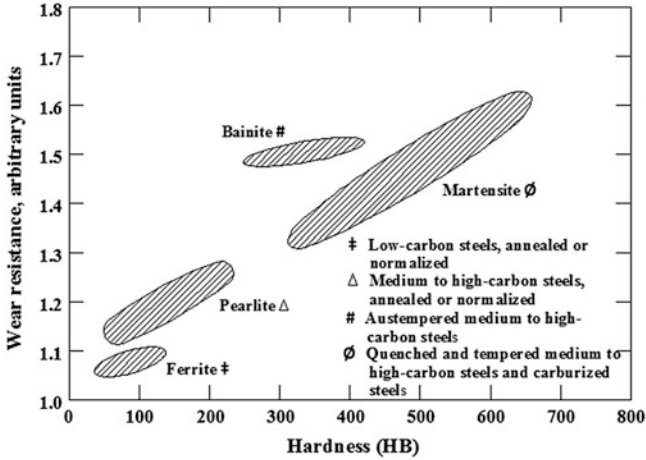


Fig. 5.15 Effect of microstructure and hardness on abrasive wear resistance of various steels [81]

$$A = k_3 \times p^2 \quad (5.12)$$

where k_3 is particle shape dependent constant. According to Brookes et al. [83] the depth of indentation is given by

$$p^2 = \frac{k_4 \times L}{H} \quad (5.13)$$

where k_4 is another constant which depends on the shape of the particle, L is the load on the particle and H is the hardness of the contacting surface. Now the mean load on the particle is

$$\bar{L} = \frac{\sigma}{N} \quad (5.14)$$

where σ is the applied load per unit area and N is the number of contacting particles per unit area and is given as

$$N = \frac{k_5}{d^2} \quad (5.15)$$

where k_5 is a constant and d is mean particle diameter. From Eqs. (5.13)–(5.15) the following equation can be obtained:

$$p \propto \frac{d}{\sqrt{\sigma H}} \quad (5.16)$$

Combining Eqs. (5.12) and (5.16) cross-sectional area of the groove is obtained as

$$A = \frac{k_6 d^2}{\sigma H} \quad (5.17)$$

Thus, volume wear (W) per unit area per unit sliding distance can be obtained as [84]

$$W = \frac{k_1 \times k_2 \times k_6 \times S}{\sigma H} \quad (5.18)$$

where k_6 is a constant. Abrasion wear resistance was found to be related to hardness of the hardfaced layer by Buchely et al. [82] as given in Fig. 5.16. This behaviour is in line with Eq. (5.18). Hardness dependence of abrasive wear rate also complies with Eq. (1.16) of Chap. 1. Similar observation is also noted by Chang et al. [85]. They deposited a series of Fe–Cr–C layers by gas tungsten arc welding (GTAW) on ASTM A-36 steel. They also used Cr and graphite filler rod. Depending on amount of graphite addition, various hypereutectic microstructure containing $(\text{CrFe})_7\text{C}_3$ carbides and eutectic colonies of $[\text{Cr-Fe} + (\text{CrFe})_7\text{C}_3]$ were obtained. With increase of carbon content, volume fraction of primary carbides $(\text{CrFe})_7\text{C}_3$ increased, their size decreased, hardness and abrasive wear resistance increased.

Similarly, Buchanan et al. [86] studied the abrasive wear behaviour of commercially available Fe–Cr–C hardfacing alloys, a hypereutectic type and a hypoeutectic type. Their result under dry sand abrasive test shown in Fig. 5.17 indicates increase in abrasive wear rate with increasing applied load in accordance with Eq. (5.18). Although there was significant difference in their hardnesses, there was no clear superiority in wear resistance under the conditions examined. However, the wear rate was not always directly proportional to load. The hypereutectic coating exhibited a transition from low to high wear coefficient when the higher loads were applied. This was due to severe fracturing of the primary carbides. The abrasion resistance of the hardfacing is determined primarily by the microstructure. On the one hand, the hypoeutectic material attained its wear resistance through the dispersion of the carbides within the matrix and its capacity to undergo strain hardening, with subsequent enhancement in its resistance to microploughing and microcutting. On the other hand, the hypereutectic resisted wear by virtue of its primary and eutectic carbides. However, the electrode coating was too enriched with carbon and chromium, producing a weld with excess carbide volume that eventually reduced wear resistance.

Bern and Fischer [87, 88] investigated 15 different commercial Fe–Cr–C hardfacing alloys containing B, Ti and Mn. They noted that the microstructure primarily consisted of solidified coarse hard phases embedded in fine eutectic of hard lamellas and metallic constituent. Depending on the $B/(B + C)$ ratio, M_3C , M_7C_3 and MC carbide-containing boron or M_2B , M_3B_2 and MB_2 boride-containing carbon were formed. MC and MB_2 hard phases contained mainly Ti. Other

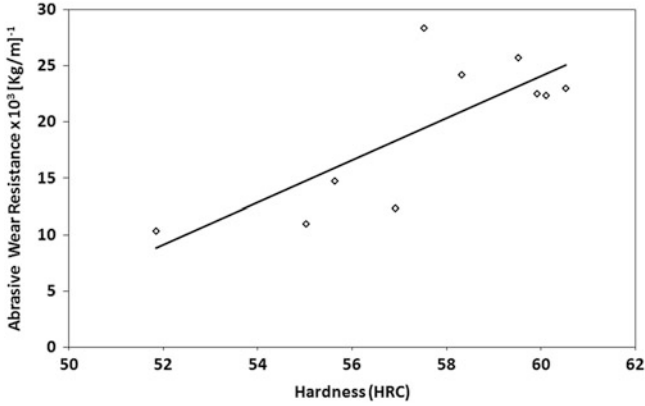


Fig. 5.16 Influence of hardness on abrasive wear resistance [82]

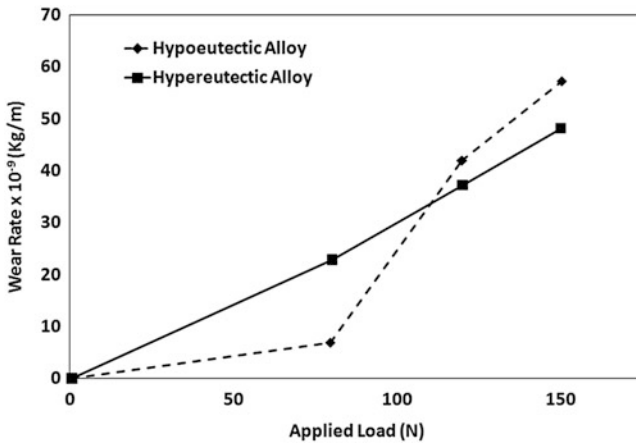


Fig. 5.17 The increase in abrasive wear rate with increasing applied load for Fe–Cr–C hardfacing alloy [86]

elements like, Cr, Fe and Mn were equally distributed in all phases and tried to increase retained austenite. Both the hardness and abrasive wear resistance increased with increase in hard phase volume fraction up to 50 % as long as hard phases were harder than the abrasives and this trend was more pronounced harder the eutectic is.

Kirchgaßner et al. [37] developed a new complex Fe–Cr–W–Mo–Nb hardfacing alloy with high boron content and compared the abrasive wear resistance of the alloy with lower alloyed hardfacing materials on base Fe–Cr–B–C, a synthetic multiphase hardfacing alloy on iron base with around 50 wt% tungsten carbides, a crack-free martensitic Fe–Cr–C hardfacing alloy containing finely precipitated niobium carbides and a conventional hypereutectic Fe–Cr–Nb–C hardfacing

alloy. Either synthetic materials using tungsten carbides or complex alloys providing both hard phases and a hard and tough nanostructured matrix at the same time performed best and their abrasive wear properties were comparable.

Similarly Dwivedi [89] found the influence of the composition and heat treatment of overlays on the abrasive wear resistance of iron base hardfacing overlays alloy. Overlays were deposited using a shielded metal arc (SMA) welding process on structural steel using two commercial hardfacing electrodes, i.e. Fe—6 % Cr—0.7 % C and Fe—32 % Cr—4.5 % C. It was found that the wear resistance of the high Cr—C coating is better than the low Cr—C hardfacing under identical conditions. Heat treatment of overlays affected wear resistance. Soaking at low temperature (503 K, 673 K) enhanced wear resistance but high temperature exposure (773 K, 873 K) adversely affected it.

The influence of welding process on the abrasive wear resistance can be obtained from the work of Coronado et al. [90]. In their research, four kinds of welding deposits applied through two different welding processes: flux cored arc welding (FCAW) and shielded metal arc welding (SMAW). The other variable of the tests was the deposited layers. The hardfacing deposits were evaluated using the dry sand—rubber wheel test rig. Their result is provided in Fig. 5.18. FCAW welds presented higher abrasive wear resistance than the SMAW deposits. The hardfacing deposit formed by uniformly distributed carbides rich in titanium presented the highest abrasive wear resistance. Abrasive wear resistance was higher when three layers were applied. The results showed that the most important variable to improve abrasion resistance is the microstructure of hardfacing deposits, where the carbides act as barriers to abrasive particle cutting. Hardfacing using FCAW presents higher abrasive wear resistance than hardfacing by SMAW process because it presents a microstructure composed of an eutectic matrix with carbides rich in titanium. Such microstructure acts as barriers to cutting by abrasive particles. The abrasive wear mechanisms found on the worn surfaces were microcutting, microploughing and wedge formation.

Metal matrix dispersed with tungsten carbide has provided hardfacing layers with the highest available resistance to abrasive wear. The main role of the carbide particles in these coatings has been to act as a wear-resistant barrier to abrasives. Accordingly, the resistance to abrasive wear of metal matrix composites has been shown to increase with the proportion of carbide phase in the metal matrix [91–93]. Badisch and Kirchgaßner [58] found that welding process parameters profoundly influence the abrasive wear rate. Weld deposit of a typical NiCrBSi hardfacing alloy reinforced with tungsten carbide obtained by plasma transfer arc at high current and high voltage by double layer deposition resulting in a high content of uniformly distributed tungsten carbides in a metal matrix gives the maximum resistance to wear in pure abrasion. In contrast, Katsich and Badisch [94] deposited a WC/W₂C-reinforced Ni-based hardfacing by plasma transferred arc (PTA) welding using different welding currents. Their investigation showed significant carbide degradation with increasing welding current, resulting in a significantly reduced primary carbide content and carbide diameter. Reduced carbide content indicated a significant wear rate increase under pure three-body abrasion

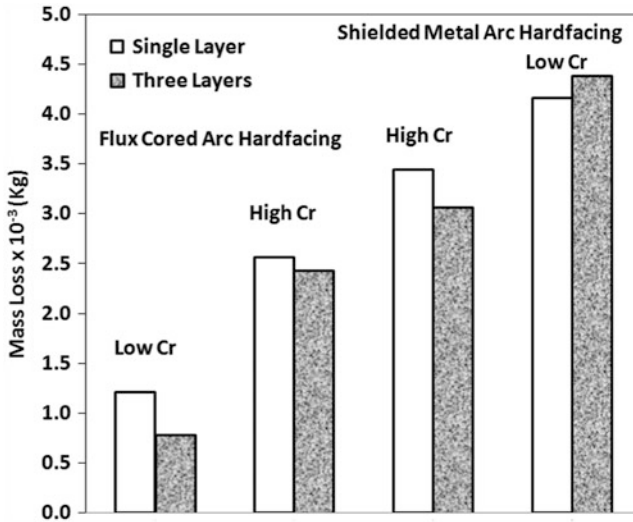


Fig. 5.18 The influence of welding process on the abrasive wear resistance [90]

conditions. The abrasive wear rate of metal matrix composites in pure abrasion has been shown to increase strongly with a rise in the level of degradation of the primary carbide during the deposition process [95, 96]. A complex high alloy deposit has shown a higher resistance to abrasive wear than either a WC or CrBC type of reinforced composite [97]. But very little data exists on the abrasive wear of hardfacing deposits of the complex high alloy type.

Carbide-containing cobalt base alloys are quite popular hardfaced layers for protection against abrasive wear. The abrasive wear rate of several standard Co-based alloys is shown in Fig. 5.19 [28]. These alloys were deposited by gas tungsten arc welding (GTAW). ERCoCr-C alloy with 26–33 wt% Cr and 11–14 wt% W exhibits the lowest abrasive wear rate. The carbon content of this alloy is over 2 % and it contains large primary carbide and Co–M₇C₃ eutectic. Alloys containing low carbon is reasonably ductile but abrasive wear resistance is low (alloy ERCoCr-E). When carbon content is increased to 1 % as in alloy ERCoCr-A and alloy ERCoCr-B, a network of Co–M₇C₃ eutectic is developed. Similarly abrasive wear rate of several Triboalloy deposited by plasma transfer arc is presented in Fig. 5.20 [28]. Although, the volume loss of Ni base alloy ERNiCr-C is the minimum, the wear rates of Triboalloys are also quite low. Among various Triboalloy, Triboalloy-800 has minimum wear rate.

The composition of the hardfaced surface also governs the abrasive wear rate. The influence of Mo content of Stellite 6 hardfaced alloy on the abrasive wear rate is shown in Fig. 5.21 due to Shin et al. [55]. The Stellite 6 hardfacing alloys with different Mo contents have been deposited on AISI 1045-carbon steel using plasma-transferred arc (PTA) welding apparatus. With an increase in Mo contents, the M₂₃C₆ and M₆C type carbides were formed instead of Cr-rich M₇C₃ and M₂₃C₆

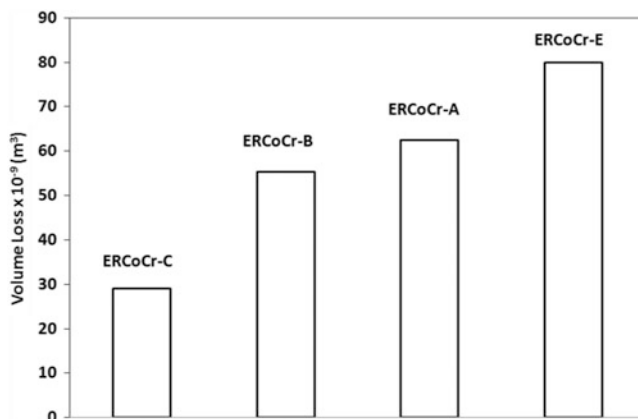


Fig. 5.19 Bar diagram showing the abrasive wear rate of a series of Co base alloys obtained by GTAW process [28]

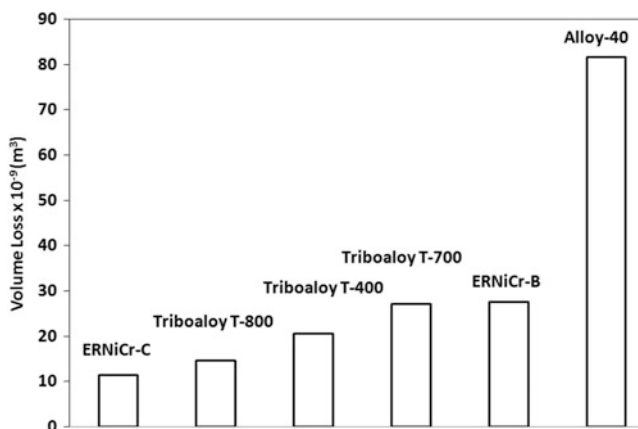


Fig. 5.20 Bar diagram showing the abrasive wear rate of a series of Co base alloys obtained by plasma transfer arc

type carbides observed in the interdendritic region of the Mo-free Stellite 6 hardfacing alloy. The size of Cr-rich carbides in interdendritic region decreased, but that of M_6C type carbide increased with the refinement of Co-rich dendrites. The volume fraction of Cr-rich carbides slightly increased, but that of M_6C type carbide abruptly increased. This microstructural change was responsible for the improvement of the mechanical properties such as hardness and wear resistance of the Mo-modified Stellite 6 hardfacing alloy. This change in mechanical properties, in turn, altered the abrasive wear rate which decreased with increase in Mo content.

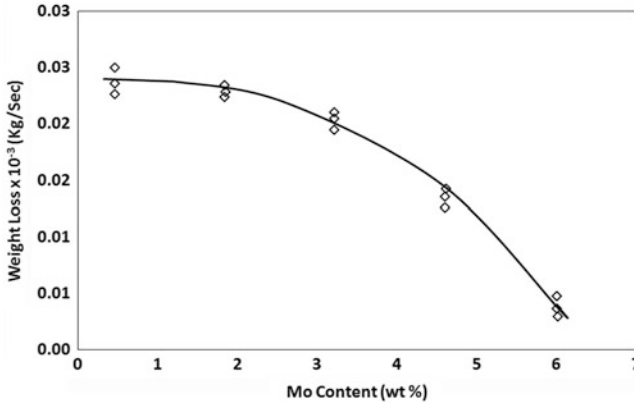


Fig. 5.21 Variation of abrasive wear as function of Mo content [55]

The relative abrasion of a series of nickel base hardfaced surfaces are illustrated in Fig. 5.22. Similar to wear, abrasion resistance of boride-containing alloys is also lower than carbide-containing alloy in general and colmonoy-6 has best abrasion resistance among boride-containing alloys. It is to be stated that unlike wear resistance, colmonoy-98 exhibits very poor abrasion resistance. Further, tungsten containing hardfaced surface also shows excellent abrasion resistance.

5.5.3 Erosive Wear

Another important tribological property for which hardfaced surfaces are used is erosive wear. Solid particle erosion behaviour of different high carbon and high chromium hardfacing electrodes deposited on grey cast iron was studied by Chatterjee and Pal [38] using quartz sand and iron ore as erodent particles. Erosion test was carried out as per ASTM G76 test method. Considerable differences in erosion rates were found among different hardfacing electrodes at normal impact. Both volume fraction of carbides and type of carbides played an important role in the erosion behaviour of the deposits when quartz sand was used as erodent particles. The erosion rate decreased with the total alloying element as shown in Fig. 5.23. On the other hand, only volume fraction of carbides irrespective of carbide type mainly controlled the erosion rate of the same deposits when iron ore was used as erodent particles. This result with iron ore particle is shown in Fig. 5.24. Such difference is attributed to the difference in metal removal mechanisms by the two erodent particles used. Hard quartz sand particles were capable of causing damage to most of the carbides while relatively softer iron ore particles were unable to fracture any carbides present in the microstructures. Furthermore, relatively brittle matrix led to high erosion rate which is significant in case of quartz sand as erodent, but not in case of iron ore particles. Hardness is

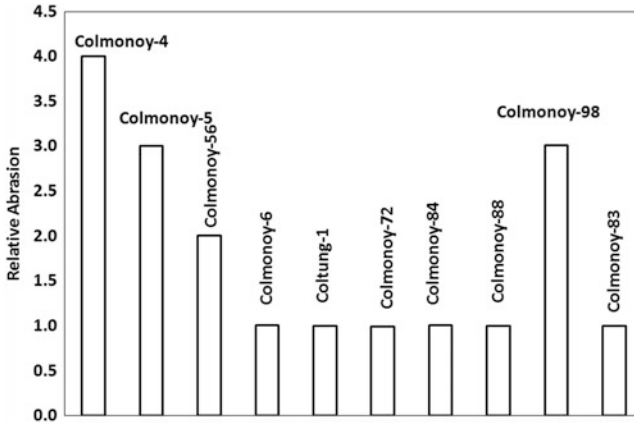


Fig. 5.22 The relative abrasion of a series of nickel base hardfaced surfaces

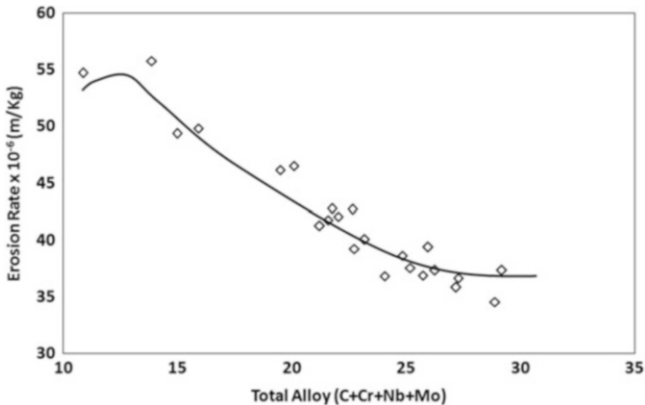


Fig. 5.23 Variation of erosion rate as function of total alloy content [38]

not a true index of erosion resistance of hardfacing deposits. Similarly Stevenson and Hutchings [98] also noted that Silica and silicon carbide erodents were able to fracture the carbide particles of hardfaced layer, whereas sinter particles were unable to cause any gross fracture of carbides in the hardfaced layer.

Sapate and Rao [99] noted that the dependence of erosion rate on impingement angle was in general weak for weld hardfacing high chromium cast iron alloys. The peak in erosion rate occurred at impingement angle of $60\text{--}90^\circ$ depending upon the alloy and the erodent particle hardness. Although the erosion rate decreased with increase of volume fraction of carbide particle [100], Sapate and Rao noted that the dependence of erosion rate on carbide volume fraction was a strong function of erodent hardness [101]. Large volume fraction of carbides proved beneficial to the erosion resistance with softer erodent particles. With silica sand particles at normal

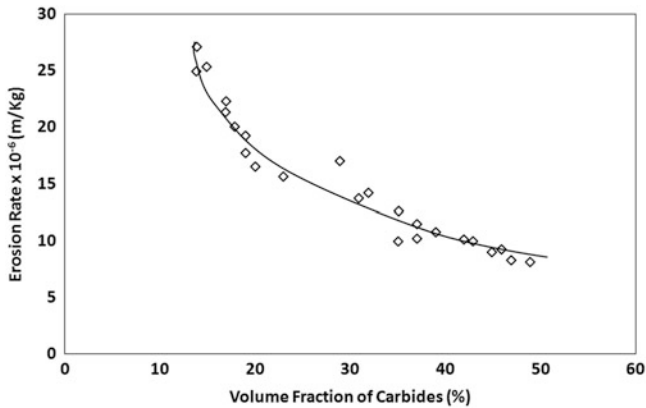


Fig. 5.24 Variation of erosion rate of high carbon high chromium hardfacing layer as function of volume fraction of carbides using iron ore as erodent [38]

impact and with alumina particles, large volume fraction of carbides were detrimental to the erosion resistance. The material removal mechanisms from the carbides were strongly influenced by the erodent particle hardness and the impingement angle. With softer erodent particles, material removal mechanism involved edge chipping whereas with harder erodent particles indentation and gross fracture was predominant erosion mechanism in addition to the edge effect.

Relative erosion of a series of nickel-based alloy shown in Fig. 5.25 indicates that these alloys are not good for erosion. In general, both boride-containing and carbide-containing alloys exhibit poor erosion resistance. However, colmonoy-98 which shows very poor abrasion resistance has excellent erosion resistance. Erosion resistance of tungsten-containing alloy is also very low.

Katsich et al. [102] designed two different types of hardfacing alloys of Fe–Cr–C incorporating Nb, Mo and B to ensure improved erosion performances at elevated temperature. Mild steel was hardfaced with these alloys under optimised gas metal arc welding (GMAW) condition. Erosive wear of these coatings was evaluated for four different temperatures, for two different impact angles and at one impact velocity. Results, as shown in Fig. 5.26 indicate that the erosion rate of these coatings increases with increase of test temperature and impact angles. Among various coatings, Fe–Cr–C coating containing higher amount of Nb, Mo and B exhibits best erosion resistance particularly at elevated temperature. SEM images showing the morphology of the eroded surface and the transverse section of eroded surface of hardfaced Fe–Cr–C alloy are shown in Fig. 5.27. Eroded surface exhibits breaking of carbide and boride hard phases. Limited cracking of the matrix can be seen as the matrix contains high amount of carbide and hence tends to exhibit brittle behaviour. Transverse section exhibits restricted cracking of hard phases and crack-free matrix. The interface between the matrix and the hard phases also appears to be excellent and consequently no pulling out of hard phases is found. Thus material loss is primarily by brittle chipping of both hard phases and hard matrix. Badisch

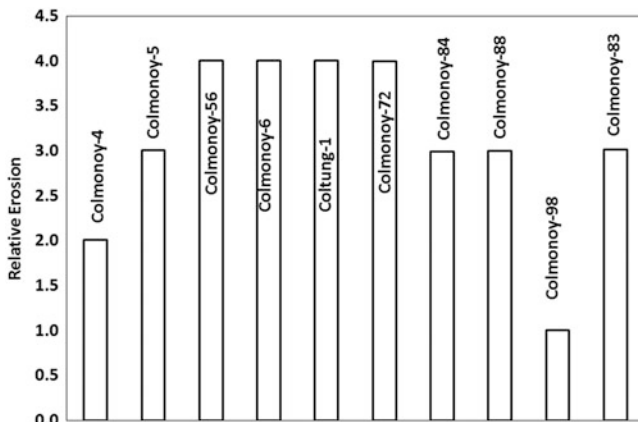


Fig. 5.25 Relative erosion rate for a series of Ni base hardfaced alloy

et al. [103] also noted that during erosion of hardfaced alloys, a coarse microstructure with carbides performs well under glancing impact angle. For Fe–Cr–C hypereutectic alloy, material removal during erosion is by breaking and pulling out of coarse hard phases. Uniform brittle chipping of hard phases and hard matrix causes material loss of Fe–Cr–B complex alloy during erosion.

Yıldızlı et al. [104] surfaced low carbon steel plates with single, double and triple pass bead on-plate welds using the shielded metal arc welding technique with high manganese electrode. The microstructure, hardness and erosive wear resistance of the surfaces were investigated. As the number of the deposit layer increased, the microstructure was found to change from martensite with retained austenite to austenite. Under the condition of erosive wear, the wear resistance of the first layer was the highest of all. Being approximately nine times higher than that of the substrate, the erosion rate of the first layer was suitable for low speed impact erosion tests. However, those of the second and the third layers tend to be arising with impact angle. Being thick and including all layers, triple hardfaced surfaces can be longer lasting in application.

5.6 Application of Hardfacing Surfaces

Hardfacing is carried out on several engineering components. Figure 5.28 illustrates hardfaced surfaces and highly loaded edges of components which are used in agricultural industry for soil treatment [105]. Application of hardfacing surfaces depends on the type of hardfacing materials. Iron-based hardfacing surfaces having pearlitic structure are used as build up of mine car wheels, shafts, rolls, cams and gears, etc. Martensitic iron-based hardfaced surfaces can be used for crane wheels, cable sleeves, undercarriage of tractors and pipe forming rolls. Some martensitic

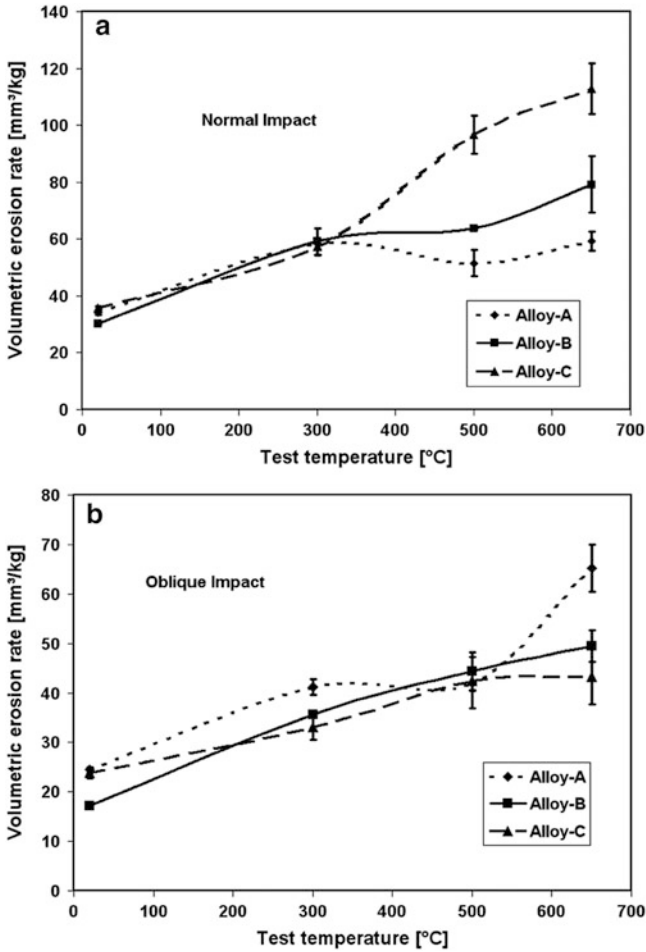
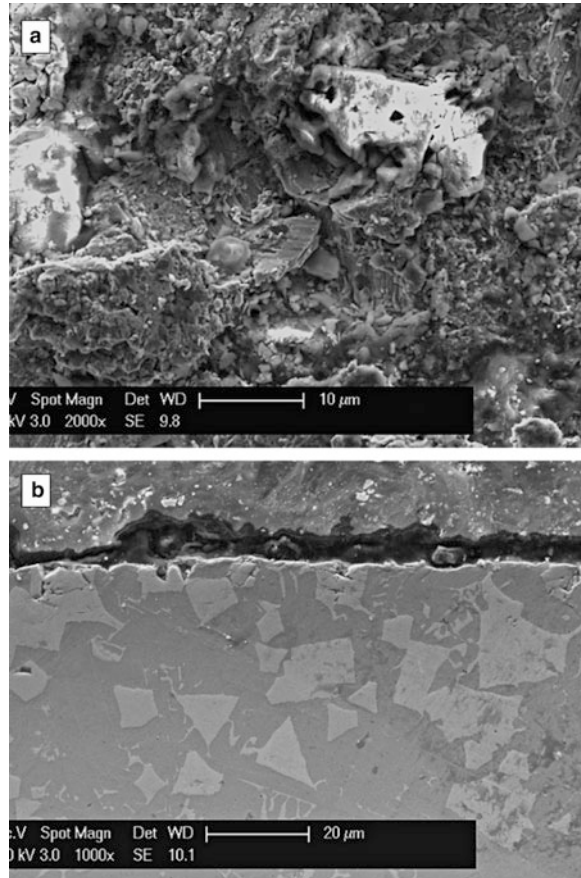


Fig. 5.26 Variation of erosion rate of iron based hardfaced surfaces with temperature under (a) normal impact and (b) oblique impact [102]

structures contain carbides making it still harder. Such surfaces are used in forging dies, shoes of pincer guide, etc. Tool steel variety of hardfaced surfaces are used for shear blades, trimming dies, cement chutes, earth moving equipment and machine tools components. Hardfaced layer with martensitic stainless steel composition and structures is used for cladding rolls of continuous caster, blast furnace bells. White iron type layers are used for protection in coal pulverising equipment, railway tracks, crushed roll shell, bucket lips, teeth and impact hammer of rock crushing and transporting system.

Cobalt base alloys such as Stellite 1 and Stellite 6 are used in seat and gates of valve, shafts and sleeves of pumps, bearings and bearing sleeves. Higher varieties of stellites are used for saw teeth, rotary slitters, cutting edges of knives of carpet,

Fig. 5.27 SEM image showing (a) the morphology of the eroded surface and (b) the transverse section of eroded surface of hardfaced Fe–C–Cr alloy [102]

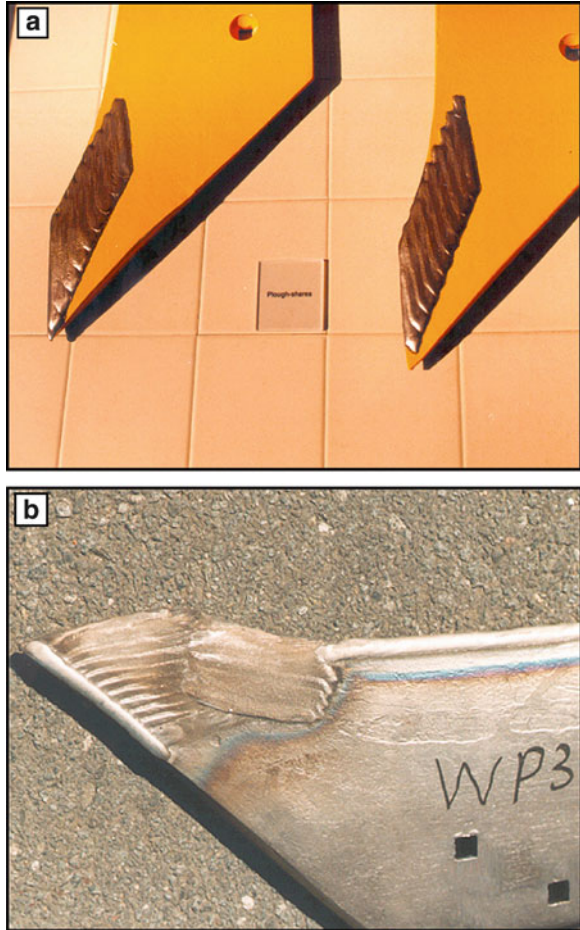


paper, plastic industries. Stellite 701, 704, 706, etc., are employed for superior wear corrosion applications such as tricone rock bits of oil drilling industries. Triboalloys are also used in application similar to satellite, e.g. mechanical seals, thrust rings, etc.

Among Ni base alloys, Deloro variety alloys are used most extensively. These alloys are used in glass forming plungers, diesel engine valves, wear rings, seal rings, dies, moulds, shafts, bearings, cylinder liner, sleeves, stem guides, etc. Colmonoy varieties of alloys are used for pumps and pumps parts, nuclear industry, plastic extrusion screws, centrifuges and wire drawing capstans. Surfaces by ERNiCr alloys can be used for trims of fluid control valve, mechanical coupling, feed screw, slurry pumps, rebuilding of hot extrusion and forging dies. An image of hardfaced cutting edge used in wood processing is given in Fig. 5.29.

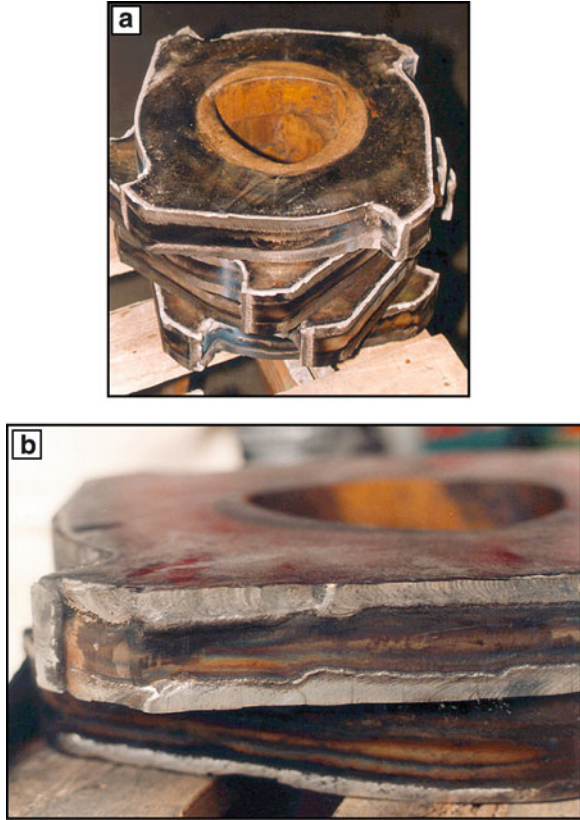
WC–Co is most widely used hardfacing material in recent time. WC–Co hardfacing is used in mining industry. Bucket wheel excavator teeth, shovel teeth, dragline teeth, dragline chain, dragline pins, undercarriage parts, dozer link pads, etc., are hardfaced with these materials in surface mining industry. For deep mining

Fig. 5.28 Images of hardfaced surfaces and highly loaded edges in agricultural industry for soil treatment [105]



activity, longwall miners, continuous miners, feeders beakers, cutter drums, crushing hammer, conveyer parts wear parts, etc., are hardfaced with WC-Co. Chutes, hammers, crushers, grinding, pulverising, wear parts and screw conveyers are some implements that are hardfaced with WC-Co. In construction industry, ground engaging tools, cutting edges, dozer blades, grader blades, trencher teeth, tunnelling equipment, wear parts, augers, dozer undercarriage parts, horizontal directional drilling equipment, etc., are hardfaced. Parts of processing industry are mixing and blending parts, screw conveyers, paddles, etc. Sugar mill rolls, sugar mill hammers, disc, injector, point subsoilers, etc., are hardfaced important agricultural equipment.

Fig. 5.29 An image of hardfaced part of cutting edge used in wood processing industry [105]



5.7 Direction of Future Research

With hectic activities in research and development on surface engineering all over the world along with the trend of function specific treatment of materials, it is expected that hardfacing will be used extensively in all related field of manufacturing industries. The prerequisite of manufacturing industries with favourable production cost is to use hardfacing as most favoured surface modification technique. Application of hardfacing has been facilitated by availability of flexible equipment. The modern trends are development of single purpose equipment capable of hardening, welding and melting, universal flexibility, adaptability to integration to flexible machine system.

Hardfacing surfaces face direct competition primarily from thermal sprayed coatings. However, hardfaced surfaces produce a diffused or remelted interface with the substrate. In recent times, wide varieties of hardfaced materials have been developed and still further development in materials front having different composition and microstructure will continue. It is imperative to generate extensive database on elevated temperature tribological properties of hardfaced surfaces. It

is equally important to carry out extensive study on the nature of interaction between corrosion and tribological degradation of hardfaced layer as the work in this direction has hardly been reported. Thin hardfaced films and application of hardfaced layer have found limited usage, the area of which should be extended. Development of various sensors related to hardfacing operation resulted in better efficiencies and process control. Further development in sensors continues giving improved life of equipment and better surfaces. Research is in progress to develop sensors for monitoring the dilution of hardfaced surfaces. Friction surfacing is another area which exhibits immense potential. Serious attempts are being made to friction surface larger variety of incompatible material and produce more variety of refined structures.

An area which deserves extensive attention is electron beam hardfacing [106]. High energy density and deep penetration capability are the main advantages of electron beam hardfacing and this puts this method ahead of laser surface modification. Thus, this method which is not finding elaborate usage should be explored for variety of materials combination for hardfacing. As this process is a high precision hardfacing process accompanied with low heat input, this process can be employed to many new applications requiring high accuracy, minimum stress and distortion.

In spite of comprehensive research work, there is still wide scope for basic research to establish the potential and limitation of existing methods in order to pave the way for further industrial applications not only in the areas of process technology but also in the areas of materials. Other factors include engineering and economic aspects.

References

1. Brienan EM, Kear BH (1983) In: Bass M (ed) Laser material processing. North Holland Publishing, Amsterdam, p 235
2. Carslaw HS, Jaeger JC (1959) Conduction of heat in solids. Oxford University Press, Oxford
3. Leshchinskiy LK, Sumotugin SS (2001) Weld J 80:25s
4. Gulenc B, Kahraman N (2003) Mater Des 24:537
5. Wilden J, Bergmann JP, Frank H (2006) J Therm Spray Technol 15:779
6. Deuis RL, Yellup JM, Subramanian C (1998) Compos Sci Technol 58:299
7. Nurminen J, Nötkki J, Vuoristo P (2009) Int J Refract Met Hard Mater 27:472
8. Man HC, Cui ZC, Yue TM, Chang FT (2003) Mater Sci Eng A 355:167
9. Wang LS, Zhu PD, Cui K (1996) Surf Coat Technol 80:279
10. Chong PH, Man HC, Yue TM (2001) Surf Coat Technol 145:136
11. Powers DE, Schumacher BW (1989) Weld J 68:48
12. Powers DE (1988) In: Metzbowner EA, Hauser D (eds) Proc. conf. power beam processing, ASM International, Ohio, pp 25–33
13. Liu Y, Sun C, Chen X (1987) Trans China Weld Inst 8:31
14. Matsui S, Matsumura H, Yasuda K (1987) Weld World 25:16
15. Franchini F (1993) Weld Int 7:206
16. Russel RJ (1980) Weld J 61:21
17. Metzger G, Lison R (1976) Weld J 55:230s

18. Bedford GM (1990) *Met Mater* 6:702
19. Vitanov VI, Voutchkov II, Bedford GM (2000) *J Mater Process Technol* 107:236
20. Li JQ, Shinoda T (2000) *Surf Eng* 16:31
21. Bedford GM, Vitanov VI, Voutchkov II (2001) *Surf Coat Technol* 141:39
22. Kaskov YM (2003) *Weld J* 82:42s
23. Kompan YY, Sufonnihov AN, Pevrov AN, Svirskii EA (1994) *Weld Int* 8:986
24. Agarwal A, Dahotre NB (1999) *J Mater Eng Perform* 8:479
25. Agarwal A, Dahotre NB (1998) *Surf Coat Technol* 106:242
26. Agarwal A, Dahotre NB (1999) *Surf Eng* 15:27
27. De A (1993) ASM handbook, vol 6, Welding brazing and soldering. ASM International Materials Park, Ohio, pp 789–807
28. Crook P, Farmer HN (1992) ASM handbook, vol 18, Friction lubrication and wear. ASM International Materials Park, Ohio, pp 758–765
29. Chandel RS (2001) *Indian Weld J* 26:33
30. Avery HS, Chapin HJ (1952) *Weld J* 31(10):917
31. Powell GLF (1979) *Aust Weld Res* 6:16
32. Gulenc B, Kahraman N (2003) *Mater Des* 24:537
33. Bayraktar E, Levaillant C, Altintas S (1993) *J Physique IV Colloque C7* 3:61
34. Pelletier JM, Oucherif F, Sallamand P, Vanes AB (1995) *Mater Sci Eng A202*:142
35. Ball A (1983) *Wear* 91:201
36. Menon R (2002) *Weld J* 81:53
37. Kirchgäßner M, Badisch E, Franek F (2008) *Wear* 265:772
38. Chatterjee S, Pal TK (2003) Wear behaviour of hardfacing deposits on cast iron. *Wear* 255:417
39. Powell GLF, Carlson RA, Randle V (1994) *J Mater Sci* 29:4889
40. Lesko A, Navera E (1996) *Mater Char* 36:349
41. Atamert S, Bhadeshia HKDH (1990) *Mater Sci Eng A* 130:101
42. Fischer A (1984) Fortschrittberichte der VDI Zeitschriften. VDI Verlag, Düsseldorf, S 69
43. Buytoz S (2006) *Mater Lett* 60:605
44. Branagan DJ, Marshall MB, Meacham BE (2005) In: Proceedings of international thermal spray conference, Basel (CD-Rom)
45. Wang XH, Zou ZD, Qu SY, Song SL (2005) *J Mater Process Technol* 168:89
46. Svensson LE, Grefott B, Ulander B, Bhadeshia HKDH (1986) *J Mater Sci* 21:1015abc
47. Lee S, Choo SH, Baek ER, Ahn S, Kim NJ (1996) *Metall Mater Trans A27*:3881
48. Kesavan D, Kamaraj M (2010) *Surf Coat Technol* 204:4034
49. Bhaduri AK, Indira R, Albert SK, Rao BPS, Jain SC, Asokkumar S (2004) *J Nucl Mater* 334:109
50. Persson DHE, Jacobson S, Hogmark S (2003) *Wear* 255:498
51. Mason SE, Rawlings RD (1994) *Mater Sci Technol* 10:924
52. Mason SE, Rawlings RD (1989) *Mater Sci Technol* 5:180
53. Johnson MP, Moorehouse P, Nicholls JR (1990) Diesel engine combustion chamber materials for heavy fuel operation. Institute of Operation, Institute of Marine Engineers, London, p 61
54. Nicholls JR (1994) *Mater Sci Technol* 10:1002
55. Shin JC, Doh JM, Yoon JK, Lee DY, Kim JS (2003) *Surf Coat Technol* 166:117
56. Wu W, Wu LT (1996) *Metall Mater Trans A27*:3639
57. Nicholls JR, Stephenson DJ (1990) Diesel engine combustion chamber materials for heavy fuel operation. Institute of Operation, Institute of Marine Engineers, London, p 47
58. Badisch E, Kirchgäßner M (2008) *Wear* 202:6016
59. Chermont JL, Osterstock F (1976) *J Mater Sci* 11:1939
60. Llo S, Just C, Badich E, Wosik J, Danninger H (2010) *Mater Sci Eng A527*:6378
61. Huang SW, Samandi M, Brandt M (2004) *Wear* 256:1095
62. Li Q, Lei TC, Chen WZ (2003) *Surf Coat Technol* 166:117

63. Hoffman JM (2010) *Mach Des* 14:5
64. Branagan DJ, Marshall MC, Meacham BE (2006) *Mater Sci Eng A* 428:116
65. Zikin A, Hussainova I, Katsich C, Badisch E, Tomastik C (2012) *Surf Coat Technol* 206:4270
66. Bayhan Y (2006) *Tribol Int* 39:570
67. Su YL, Chen KY (1997) *Wear* 209:160
68. Wang XH, Han F, Liu XM, Qu SY, Zou ZD (2008) *Mater Sci Eng A* 489:193
69. Wang XH, Han F, Qu SY, Zou ZD (2008) *Surf Coat Technol* 202:1502
70. Foroulis ZA (1984) *Wear* 96:203
71. Bhansali KJ, Miller AE (1982) *Wear* 75:241
72. Persson DHE, Jacobson S, Hogmark S (2003) *J Laser Appl* 15:115
73. Kim CK, Lee S, Jung JY, Ahn S (2003) *Mater Sci Eng A* 349:1
74. Choo SH, Kim CK, Euh K, Lee S, Jung J-Y, Ahn S (2000) *Metall Mater Trans* 31A:3041
75. Lee S, Choo S-H, Baek E-R, Ahn S, Kim NJ (1996) *Metall Mater Trans* 27A:3881
76. Wu W, Wu LT (1996) *Metall Mater Trans* 27A:3639
77. Lee KY, Kim GG, Kim JH, Lee SH, Kim SJ (2007) *Wear* 262:845
78. Lee KY, Lee SH, Kim Y, Hong HS, Oh YM, Kim SJ (2003) *Wear* 255:481
79. Kotecki DJ, Ogborn JS (1995) *Weld J* 74(8):269s
80. Kim HJ, Yoon BH, Lee CH (2002) *Wear* 249:846
81. Ghar Z (1971) *Met Prog* Sept:46
82. Buchely MF, Gutierrez JC, Leon LM, Toro A (2005) *Wear* 259:52
83. Brookes CA, Green P, Harrison PH, Moxley B (1972) *J Phys D* 5:1284
84. Moore MA (1980) In: Rigney DA (ed) *Fundamental of friction and wear*. ASTM, Materials Park, OH, p 73
85. Chang CM, Chen YC, Wu W (2010) *Tribol Int* 43:929
86. Buchanan VE, Shipway PH, McCartney DG (2007) *Wear* 263:99
87. Berns H, Fischer A (1985) In: *Proceedings of the fifth international conference on wear of materials*, Vancouver, BC, pp 625–633
88. Berns H, Fischer A (1983) In: Ludema KC (ed) *Proceedings of the fourth international conference on wear of materials*, *Wear of materials*. ASME, New York, pp 298–302
89. Dwivedi DK (2004) *Mater Sci Technol* 20:1326
90. Coronado JJ, Caicedo HF, Gomez AL (2009) *Tribol Int* 42:745
91. Berns H, Fischer A (1987) *Metallography* 20:401
92. Berns H (2003) *Wear* 254:47
93. Simm W, Freti S (1989) *Wear* 129:105
94. Katsich C, Badisch E (2011) *Surf Coat Technol* 206:1062
95. Berns H, Fischer A (1986) *Wear* 112:163
96. Eroglu M, Zdemir NO (2002) *Surf Coat Technol* 154:209
97. Huang Z, Hou Q, Wang P (2008) *Surf Coat Technol* 202:2993
98. Stevenson ANJ, Hutchings IM (1995) *Wear* 186–187:150
99. Sapate SG, Rama Rao AV (2006) *Tribol Int* 39:206
100. Flores JF, Neville A, Kapur N, Gnanavelu A (2009) *Wear* 267:213
101. Sapate SG, Rama Rao AV (2004) *Wear* 256:774
102. Katsich C, Badisch E, Roy M, Heath GR, Franek F (2009) *Wear* 267:1856
103. Badisch E, Katsich C, Winkelmann H, Franek F, Roy M (2010) *Tribol Int* 43:1234
104. Yıldızlı K, Eroglu M, Karamz MB (2007) *Surf Coat Technol* 201:7166
105. Castolino Eutectic company brochures
106. Soon Z, Karppi R (1996) *J Mater Process Technol* 59:257